nature communications

Article

https://doi.org/10.1038/s41467-024-53404-0

OTUD5 promotes end-joining of deprotected telomeres by promoting ATM-dependent phosphorylation of KAP1^{S824}

Received: 15 December 2023

Accepted: 8 October 2024

Published online: 17 October 2024

Check for updates

Shiu Yeung Lam[1,2], Ruben van der Lugt[1,2], Aurora Cerutti[1], Zeliha Yalçin[1], Alexander M. Thouin[1], Marco Simonetta[1] & Jacqueline J. L. Jacobs[1]

Appropriate repair of damaged DNA and the suppression of DNA damage responses at telomeres are essential to preserve genome stability. DNA damage response (DDR) signaling consists of cascades of kinase-driven phosphorylation events, fine-tuned by proteolytic and regulatory ubiquitination. It is not fully understood how crosstalk between these two major classes of post-translational modifications impact DNA repair at deprotected telomeres. Hence, we performed a functional genetic screen to search for ubiquitin system factors that promote KAP1^{S824} phosphorylation, a robust DDR marker at deprotected telomeres. We identified that the OTU family deubiquitinase (DUB) OTUD5 promotes KAP1^{S824} phosphorylation by facilitating ATM activation, through stabilization of the ubiquitin ligase UBR5 that is required for DNA damage-induced ATM activity. Loss of OTUD5 impairs KAP1^{S824} phosphorylation, which suppresses end-joining mediated DNA repair at deprotected telomeres and at DNA breaks in heterochromatin. Moreover, we identified an unexpected role for the heterochromatin factor KAP1 in suppressing DNA repair at telomeres. Altogether our work reveals an important role for OTUD5 and KAP1 in relaying DDR-dependent kinase signaling to the control of DNA repair at telomeres and heterochromatin.

Under constant exposure to both environmental and endogenous sources of DNA damage, efficient repair of DNA lesions is essential to the maintenance of genome integrity[1]. Paradoxically, in particular genomic contexts, such as telomeres, activation of DNA repair mechanisms instead leads to chromosomal aberrations and genomic instability[2]. Telomeres are specialized nucleoprotein structures located at the natural ends of chromosomes. They consist of kilobases of TTAGGG DNA repeats and serve to counteract the gradual erosion of chromosomal ends upon each cycle of DNA replication[3,4]. Telomeres are bound and protected by shelterin, a six-unit protein complex that prevents misrecognition of telomeres as DNA double-strand breaks (DSBs) and unwanted activation of DNA repair pathways[5–8]. Shelterin blocks DDR signaling and DNA repair in large part through promoting the formation of a telomere-loop (t-loop) and inhibiting the accessibility of telomeric DNA to components of the DDR machinery[9]. In the absence of shelterin function, deprotected telomeric DNA ends trigger DDR signaling that induces both cellular senescence and DNA repair reactions that result in chromosome end-to-end fusions[8,10]. Such fusions are a major threat to chromosomal stability, particularly in cells escaping from senescence.

The signaling pathways involved in the DDR at dysfunctional telomeres share significant similarities with that of DNA DSBs. The DDR is initiated by the recognition of DSBs or deprotected telomeres by the MRE11-RAD50-NBS1 (MRN) complex, followed by the activation of ATM, the primary kinase responsible for DDR signaling in DSB repair[11,12]. While the precise mechanisms underlying ATM activation are still not fully understood, activated ATM phosphorylates several downstream targets, including p53, CHK2, H2A.X, and KAP1 (also known as TRIM28 or

[1]Division of Oncogenomics, The Netherlands Cancer Institute, Amsterdam, The Netherlands. [2]These authors contributed equally: Shiu Yeung Lam, Ruben van der Lugt. e-mail: j.jacobs@nki.nl

TIF1B)[13–16]. These phosphorylation events lead to cell cycle arrest, local chromatin remodeling, and recruitment of essential repair factors, ultimately enabling the repair process. In particular, phosphorylation of KAP1 has been shown to be functionally indispensable for the repair of DSBs, specifically at heterochromatin[17,18]. KAP1, in its native, SUMOylated state, serves as a critical heterochromatin scaffolding factor that promotes transcriptional repression and chromatin condensation via its interaction with various chromatin remodelers. In the presence of DSBs, the normally SUMOylated KAP1 is phosphorylated by ATM in a manner facilitated by 53BP1, RNF8 and MDC1, and exhibiting a pan-nuclear phosphorylation pattern[18]. Phosphorylation of KAP1 triggers temporary decompaction of heterochromatin in a CHD3-dependent manner, and facilitates DNA repair in an otherwise restrictive environment[19].

While the DDR signaling cascade is primarily dictated by the flow of signals in the form of protein phosphorylation, post-translational modifications by ubiquitination streamlines DDR signaling by orchestrating protein turnover, chromatin remodeling, and recruitment of repair factors[20–23]. Accordingly, key roles in the DDR have been assigned to multiple ubiquitin-system factors. However, the full complexity of how the phosphorylation and ubiquitination systems together orchestrate the DDR, and especially at telomeres, is still unknown. Here we addressed this by performing a functional genetic screen targeted at identifying ubiquitin system factors that promote DDR activation at deprotected telomeres, using ATM-dependent phosphorylation of KAP1 at its Ser-824 residue (KAP1^{S824}) as the readout.

Through this screen, we identified the OTU-family deubiquitinase (DUB) OTUD5 as a promoter of DDR activation at deprotected telomeres. OTUD5 is a phospho-activated DUB that preferentially cleaves K48- and K63-linked poly- and di-ubiquitin chains in vitro[24]. Together with the ubiquitin ligase UBR5, OTUD5 has been linked to the process of transcriptional suppression at damaged chromatin but has so far not been directly implicated in the regulation of DDR signaling and DNA repair at telomeres[25].

We find that OTUD5 promotes ATM-mediated phosphorylation of KAP1^{S824} in response to telomere deprotection, as well as in response to genome-wide, ionizing radiation (IR)-induced DNA damage. This is dependent on the ability of OTUD5 to stabilize UBR5, previously implicated in ATM activation by alleviating ATMIN-dependent inhibition on ATM in response to DSBs[26]. In addition to its role in promoting the signaling axis of the DDR, we found that OTUD5 promotes the efficiency of DNA repair exclusively at telomeres and heterochromatin, but not in general, non-specific chromatin contexts. Such facilitation is independent of ATM-driven recruitment of 53BP1 and RIF1, as the localization of these NHEJ factors to deprotected telomeres is either unaffected or only marginally compromised upon loss of OTUD5. Instead, we reveal that defective KAP1^{S824} phosphorylation is the crucial underpinning step that hinders DNA repair at telomeres in cells lacking OTUD5, as ectopic expression of phosphomimic KAP1^{S824D} is sufficient to restore telomeric NHEJ in OTUD5-depleted cells. This shows that the residual ATM activity in OTUD5-deficient cells is inadequate to support sufficient phosphorylation of KAP1^{S824}, a key step in DNA repair in KAP1-rich genomic environments such as the telomeres and heterochromatin, thereby translating into a repair defect specifically in these regions. Moreover, by genetic inactivation of KAP1, we identify an unanticipated role for KAP1 in telomere protection by restricting NHEJ at deprotected telomeres.

Altogether, our work identifies OTUD5 as a key contributor to DDR signaling and DNA repair at deprotected telomeres and heterochromatin and points at KAP1 as a critical determinant of end-joining mediated repair efficiency at dysfunctional telomeres.

Results

A functional genetic screen identifies ubiquitin system factors that promote DDR activation at deprotected telomeres

In mammalian cells, loss of function of TRF2, a core component of the shelterin complex, causes telomere deprotection, triggering DDR signaling at telomeres. A well-characterized experimental system for studying DDR activities at telomeres is a *Trf2*$^{-/-}$;*p53*$^{-/-}$ mouse embryonic fibroblast (MEF) cell line that expresses the temperature-sensitive TRF2^{I468A} mutant (TRF2ts)[27]. At the permissive temperature (32 °C), TRF2ts functionally complements the loss of endogenous TRF2 and keeps telomeres in a protected state. However, at non-permissive temperatures (37–39 °C) TRF2ts is inactivated, causing rapid and synchronous telomere deprotection and telomere-specific DDR activation (Fig. 1a). We exploited this system to gain understanding on the requirements of ubiquitin system factors for efficient DDR activation at deprotected telomeres. We designed a fluorescence-activated cell sorting (FACS)-based functional genetic screen in TRF2ts MEFs that allows identification of factors with a critical role in the activation of DDR signaling at deprotected telomers, so-called activators of the telomere damage response (ATD). To circumvent complications to DDR dynamics from cells being in different cell cycle phases, we used TRF2ts MEFs modified with the Fluorescent Ubiquitination-based Cell Cycle Indicator (FUCCI) system[28] to isolate G1 cells for detection of DDR activation.

DDR signaling at TRF2-deprotected telomeres is by at large an ATM kinase-dependent process[5]. Amongst ATM substrates, pKAP1^{S824} is strongly induced by telomere deprotection in TRF2ts MEFs[27,29]. This induction is also readily detectable by FACS, where a significant upshift in pKAP1^{S824} intensity could be detected after incubating TRF2ts MEFs at 39 °C for 3 h (Fig. 1b). To validate the specificity of pKAP1^{S824} detection by FACS, we pretreated TRF2ts MEFs with an ATM inhibitor or short hairpin RNA (shRNA) against ATM, before subjecting the cells to telomere deprotection (Fig. 1c, d). Indeed, ablation of ATM activity abolishes induction of pKAP1^{S824} by telomere deprotection. This reinforces that our FACS detection strategy specifically detects ATM-dependent KAP1^{S824} phosphorylation at deprotected telomeres.

To conduct the screen, we infected TRF2ts-FUCCI MEFs in triplicate with a lentiviral library of 609 shRNAs (pLKO.1-Puro) that target 123 ubiquitin system factors in mouse (Fig. 1e). By FACS, we selected the top 5% G1 cells with lowest pKAP1^{S824} signal after telomere deprotection for 3 h at 39 °C (Fig. 1e, Supplementary Fig. 1a). From this population displaying impaired pKAP1^{S824} induction we extracted genomic DNA, recovered shRNA sequences by PCR, and determined the enrichment of shRNAs in this population, relative to the untreated control cell population, by next generation sequencing and MaGECK-RRA analysis[30]. Significantly enriched shRNA targets point at gene candidates that are required for DDR activation following telomere deprotection.

The ATD screen identified UBE2D3, UBE2M and OTUD5 as the top three ubiquitin system factors that promote KAP1^{S824} phosphorylation at deprotected telomeres (Fig. 1f). UBE2D3 is a ubiquitin-conjugating E2 enzyme of the UBE2D enzyme family that we recently found to affect KAP1^{S824} phosphorylation in an independent study[31], and hence represents an internal positive control. UBE2M is an E2 enzyme of both the ubiquitination and neddylation system, while OTUD5, also known as DUBA, is a DUB of the OTU (ovarian tumor) deubiquitinase family.

For validation, we individually depleted UBE2D3, UBE2M or OTUD5 in TRF2ts MEFs with multiple independent shRNAs that were included in the screen and subjected them to telomere deprotection. Indeed, depletion of all three targets significantly impaired KAP1^{S824} phosphorylation upon telomere deprotection (Fig. 1g, h, Supplementary Fig. 1b, c). Due to the heavy involvement of UBE2M in the neddylation pathway (being one of only two described E2 enzymes of the neddylation system)[32], this study's focus on ubiquitination system factors, and given that E2 enzymes in general have more cellular targets than DUBs, we chose to further investigate the role of OTUD5.

OTUD5 promotes ATM-dependent DDR signaling

For more specific and robust depletion of OTUD5 in mechanistic studies we continued using CRISPR/Cas9-mediated gene knockout

https://doi.org/10.1038/s41467-024-53404-0

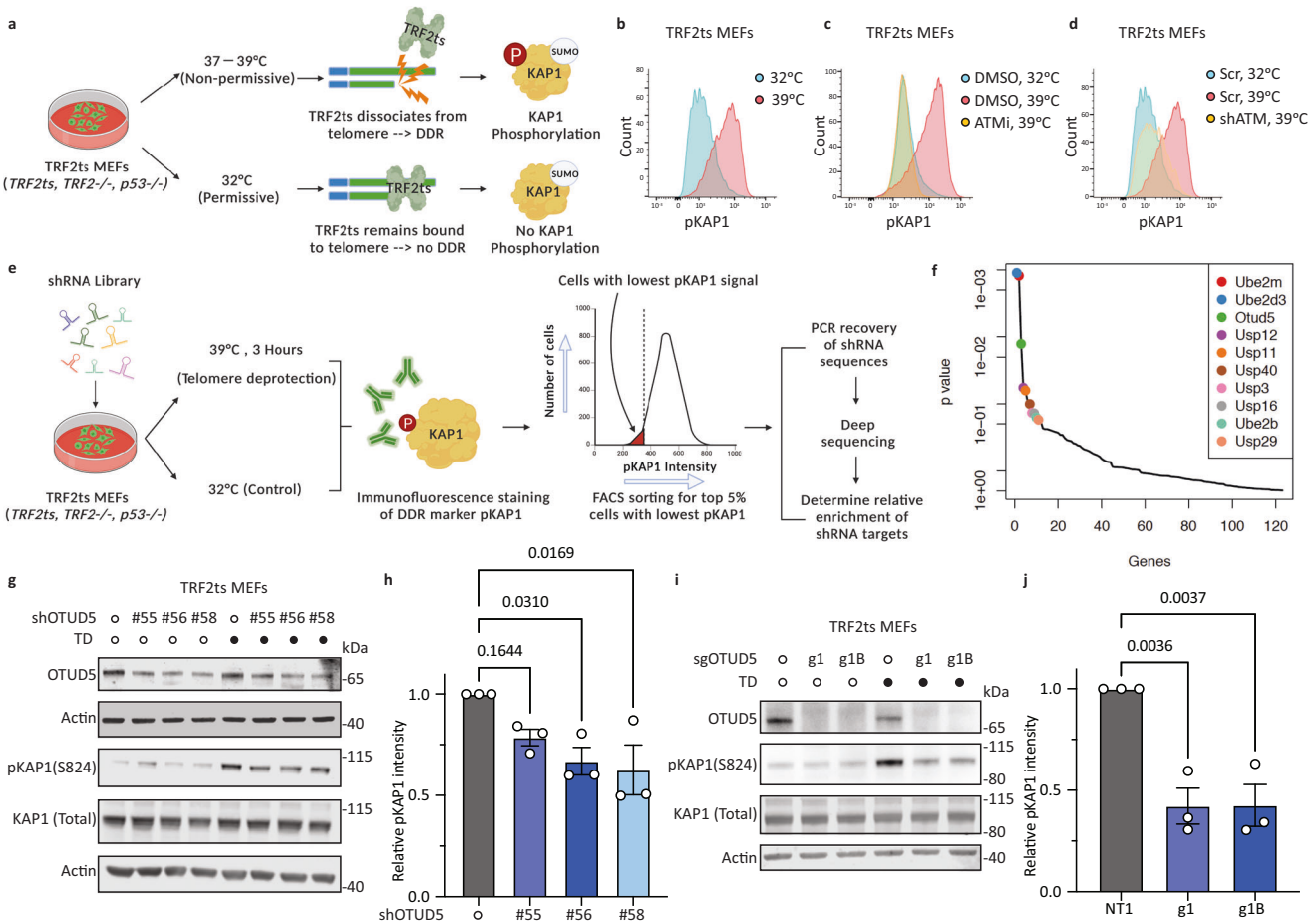

Fig. 1 | ATD screen reveals ubiquitin system factors that promote KAP1^{S824} phosphorylation upon telomere deprotection. a Schematic illustration of temperature-dependent telomere deprotection and telomeric DDR activation in TRF2ts MEFs. Created with BioRender.com released under a Creative Commons Attribution-NonCommercial-NoDerivs 4.0 International license (**b**) Assessment of pKAP1^{S824} in TRF2ts MEFs with (39 °C, 3 h) or without (32 °C) telomere deprotection by immunofluorescent staining of pKAP1^{S824} detected by FACS. **c** Assessment of pKAP1^{S824} in TRF2ts MEFs pretreated with DMSO or ATM inhibitor (ATMi), with (39 °C, 3 h) or without (32 °C) telomere deprotection. For ATM inhibition, cells were pretreated with 10 µM KU-55933 30 min before telomere deprotection. **d.** Assessment of pKAP1^{S824} in ATM-depleted TRF2ts MEFs (shATM) and control (shScr), with (39 °C, 3 h) or without (32 °C) telomere deprotection. **e** Workflow of the ATD screen. Created with BioRender.com released under a Creative Commons Attribution-NonCommercial-NoDerivs 4.0 International license. **f** Graphical representation of gene ranking of the ATD screen generated by MAGeCK-RRA analysis. A full list of hits and corresponding p-values is included in Supplementary Data 1. **g** Immunoblot analysis of pKAP1^{S824} in OTUD5-depleted TRF2ts MEFs (shOTUD5 #55/#56/#58) and control (shScramble), untreated or treated with telomere deprotection (TD; 39 °C, 3 h). Actin serves as loading control. Representative blot from three independent experiments. **h** Quantification of pKAP1^{S824} intensities in (**g**). Relative pKAP1 intensities were obtained by first correcting pKAP1^{S824} intensities to the respective total KAP1 levels, followed by a normalization to the corrected pKAP1^{S824} intensity in control (shScramble). Bars represent means ± SEM. Each dot represents one of three independent experiments. Statistical analysis was performed according to one-way ANOVA with Dunnett's multiple comparisons test. **i** Immunoblot analysis of pKAP1^{S824} in OTUD5-depleted TRF2ts MEFs (sgOTUD5 g1/g1B) and control (sgNT1), untreated or treated with telomere deprotection (TD; 37 °C, 3 h). Actin serves as loading control. Representative blot from three independent experiments. **j** Quantification of pKAP1^{S824} intensities in (**i**). Relative pKAP1 intensities were obtained by first correcting pKAP1^{S824} intensities to the respective total KAP1 levels, followed by a normalization to the corrected pKAP1^{S824} intensity in control (sgNT1). Bars represent means ± SEM. Each dot represents one of three independent experiments. Statistical analysis was performed according to one-way ANOVA with Dunnett's multiple comparisons test. Source data are provided as a Source Data file.

approaches[33]. Depletion of OTUD5 in TRF2ts MEFs with 2 independent sgRNAs (g1, g1B) recapitulated the pKAP1^{S824} defect observed with shRNA-mediated knockdown of OTUD5 (Fig. 1i, j). To address whether contribution of OTUD5 to DDR activation extends beyond a telomeric context, we challenged OTUD5-depleted human U2OS cells with ionizing radiation (IR) to induce genome-wide DSBs. Similar to its role in the response to deprotected telomeres, we found that OTUD5 is also required for robust KAP1^{S824} phosphorylation in response to genome-wide DNA damage, as IR-induced KAP1^{S824} phosphorylation was significantly reduced in OTUD5-depleted cells (Fig. 2a, b).

We then investigated the mechanism underpinning the requirement of OTUD5 for robust KAP1^{S824} phosphorylation. We observed that in addition to pKAP1^{S824}, phosphorylation of other ATM kinase substrates, including pCHK2^{T68} and γH2A.X, were also reduced upon loss of OTUD5 (Fig. 2c), suggesting that ATM activity is compromised in absence of OTUD5. In line with this, autophosphorylation of ATM on Ser-1981 (pATM^{S1981}), indicative of active ATM kinase, was significantly reduced in OTUD5-depleted U2OS cells and TRF2ts MEFs, while total ATM levels remained unaltered (Fig. 2c, d, Supplementary Fig. 2a). This suggests that OTUD5 promotes ATM activation, and thereby supports phosphorylation of its downstream targets, including KAP1, in the DDR signaling cascade.

The Ser-177 and Cys-224 residues of OTUD5 are critical to its phospho-activation and catalytic activity, respectively[24]. To assess the importance of these functional aspects of OTUD5 in promoting KAP1^{S824} phosphorylation, we performed complementation experiments with

https://doi.org/10.1038/s41467-024-53404-0

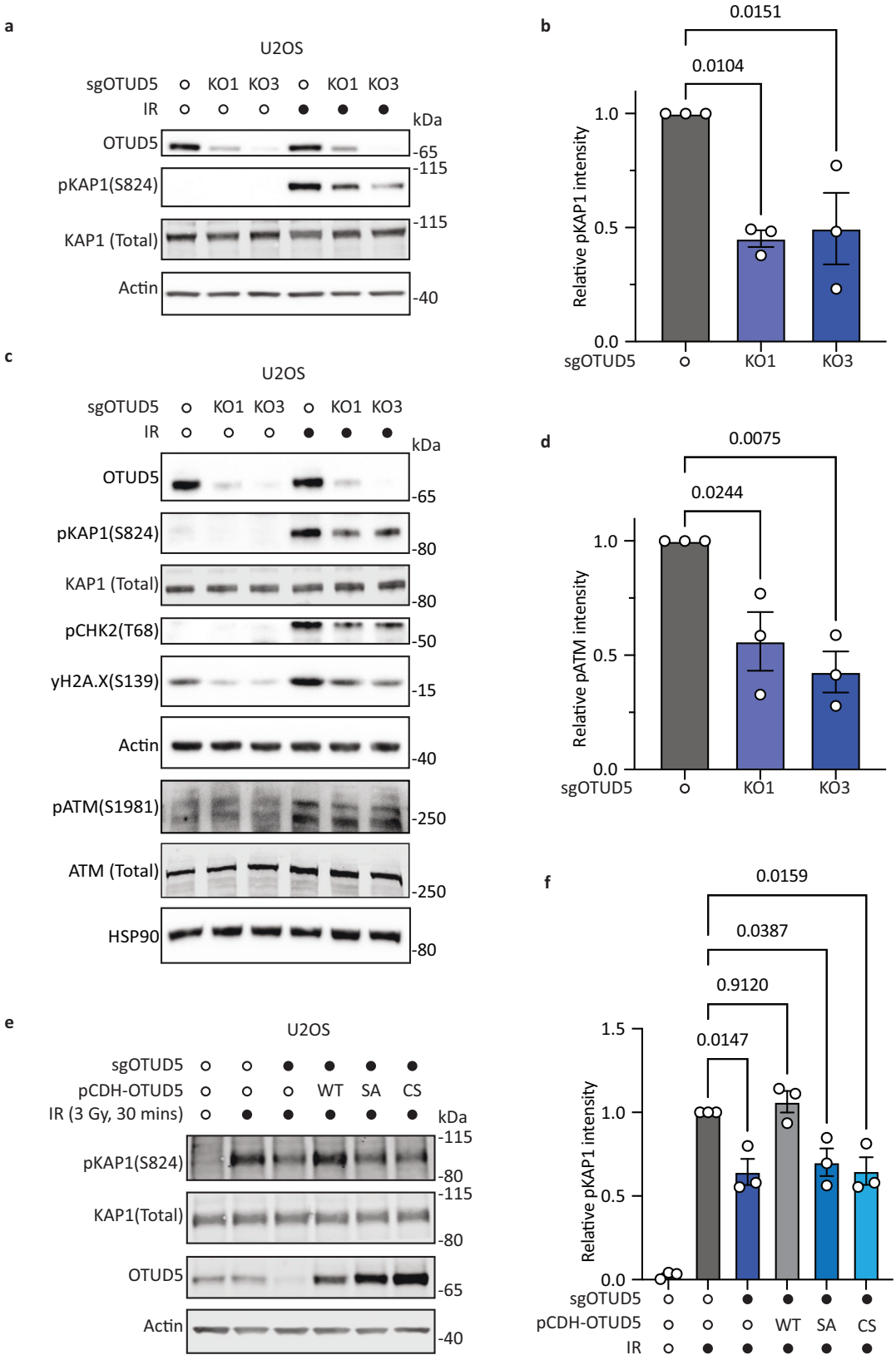

ectopic expression of OTUD5^{WT}, OTUD5^{S177A} or OTUD5^{C224S}. While expression of sgRNA-resistant, codon-optimized OTUD5^{WT} cDNA restored KAP1^{S824} phosphorylation in OTUD5-depleted cells, both OTUD5^{S177A} and OTUD5^{C224S} expression failed to do so (Fig. 2e, f, Supplementary Fig. 2b). Thus, both the DUB activity and the phospho-activation of OTUD5 are required for ATM-dependent DDR signaling.

OTUD5 promotes end-joining mediated fusion of dysfunctional telomeres

Loss of shelterin factor TRF2 results in processing of the deprotected telomeres by ligase IV- and Ku-dependent classical non-homologous end-joining (NHEJ), giving rise to chromosome-type telomere fusions (abbreviated here as chromosome fusions)[34,35]. These fusions are

Fig. 2 | OTUD5 promotes KAP1^{S824} phosphorylation by enhancing ATM activation. a Immunoblot analysis of pKAP1^{S824} levels in OTUD5-depleted U2OS (sgOTUD5 KO1/KO3) and control (sgNT1), untreated or treated with ionizing radiation (IR; 3 Gy, 30 min recovery at 37 °C). Actin serves as loading control. Representative blot from three independent experiments. **b** Quantification of pKAP1^{S824} intensity in (**a**). Relative pKAP1 intensities were obtained by first correcting pKAP1^{S824} intensities to the respective total KAP1 levels, followed by a normalization to the corrected pKAP1^{S824} intensity in control (sgNT1). Bars represent means ± SEM. Each dot represents one of three independent experiments. Statistical analysis was performed according to one-way ANOVA with Dunnett's multiple comparisons test between samples. **c** Immunoblot analysis of pATM^{S1981} and downstream phosphosubstrates of ATM in OTUD5-depleted U2OS (sgOTUD5 KO1/KO3) and control (sgNT1), untreated or treated with ionizing radiation (IR; 3 Gy, 30 min recovery at 37 °C). Actin and HSP90 serve as loading controls. Representative blot from three independent experiments. **d** Quantification of pATM^{S1981} intensity in (**c**). Relative pATM^{S1981} intensities were obtained by first correcting pATM^{S1981} intensities to the respective total ATM levels, followed by a normalization to the corrected pATM^{S1981} intensity in control (sgNT1). Bars represent means ± SEM. Each dot represents one of three independent experiments. Statistical analysis was performed according to one-way ANOVA with Dunnett's multiple comparisons test between samples. **e** Immunoblot analysis of pKAP1^{S824} levels in control (sgNT1) and OTUD5-depleted (sgOTUD5 KO3) U2OS complemented with either empty-vector, wild-type OTUD5 (WT), phospho-dead mutant OTUD5^{S177A} (SA) or catalytic-dead mutant OTUD5^{C224S} (CS) delivered with pCDH-Puro expression vector. Cells were untreated or treated with ionizing radiation (IR; 3 Gy, 30 min recovery at 37 °C) as indicated. Actin serves as loading control. Representative blot from three independent experiments. **f** Quantification of pKAP1^{S824} intensity in (**e**). Relative pKAP1^{S824} intensities were obtained by first correcting pKAP1^{S824} intensities to the respective total KAP1 levels, followed by a normalization to the corrected pKAP1^{S824} intensity in control (sgNT1, IR-treated). Bars represent means ± SEM. Each dot represents one of three independent experiments. Statistical analysis was performed according to one-way ANOVA with Dunnett's multiple comparisons test between samples. Source data are provided as a Source Data file.

generated primarily in G1 phase and appear in metaphase spreads as end-to-end fusions of both sister chromatids of one chromosome to the sister chromatids of another chromosome. As OTUD5 is required for robust DDR activation at deprotected telomeres, we assessed whether telomeric NHEJ also requires OTUD5. Indeed, depletion of OTUD5 significantly reduced the frequency of NHEJ-mediated chromosome end-to-end fusions upon telomere deprotection in TRF2ts MEFs, albeit to a lesser extent than direct inhibition of ATM with an ATM inhibitor (KU-55963) (Fig. 3a, b). This indicates that OTUD5 is required for efficient NHEJ at telomeres. To address whether OTUD5 is required for NHEJ at deprotected telomeres similarly in human cells, we depleted OTUD5 in HeLa cells harboring a doxycycline-inducible shRNA against TRF2, where telomere deprotection can be induced by doxycycline treatment[36]. Consistent with our results in TRF2ts MEFs, ablation of OTUD5 in these HeLa cells significantly reduced both telomere fusions and KAP1^{S824} phosphorylation upon doxycycline-induced TRF2 loss (Fig. 3c, Supplementary Fig. 3a, b). Furthermore, the defect in telomeric NHEJ observed in OTUD5-depleted cells is not attributable to aberrant cell cycle progression, as OTUD5 depletion did not significantly perturb cell cycle distribution under unchallenged or telomere deprotection conditions (Supplementary Figs. 3c and 4a).

Besides via classical NHEJ, deprotected telomeres can also be fused by microhomology mediated end-joining (MMEJ). This is apparent in the absence of the core NHEJ factor Ku70 and, in particular, when not only the function of TRF2 is lost but also that of TRF1[10]. To assess the impact of OTUD5 on telomeric MMEJ, we depleted OTUD5 in *Trf1$^{F/F}$;Trf2$^{F/F}$;Ku70$^{-/-}$;p53$^{-/-}$;Cre-ER^{T2}* MEFs, and induced telomere deprotection by Cre-mediated deletion of TRF1 and TRF2. Although to a lesser extent than NHEJ-mediated fusions, also MMEJ-mediated chromosome fusions were significantly reduced in OTUD5-deficient cells (Fig. 3d, e, Supplementary Fig. 3d, e). Taken together, we conclude that OTUD5 is required both for efficient NHEJ and for efficient MMEJ at deprotected telomeres.

Having established that OTUD5 promotes DNA repair by NHEJ and MMEJ at telomeres, we assessed if the role of OTUD5 in DNA repair extends beyond a telomeric context, especially since we found OTUD5 to promote both telomere-specific and genome-wide DDR activation in mouse and human cells. To determine the requirement of OTUD5 for end-joining mediated DNA repair in a genome-wide context, we assessed its impact on the NHEJ-dependent integration of a linearized plasmid, randomly into the genome of U2OS cells[37]. Unlike loss of MAD2L2, a well-established factor that promotes NHEJ both at telomeres and genome-wide[29], loss of OTUD5 did not significantly compromise NHEJ in this assay (Fig. 3f, g). In addition, we assessed the contribution of OTUD5 to NHEJ outside of a telomeric context in HEK293T cells harboring a NHEJ-HR dual reporter system, in which the efficiency of NHEJ can be measured by FACS[38]. Again, loss of OTUD5 did not significantly reduce NHEJ efficiency, in agreement with the results of the random plasmid integration assay (Fig. 3h, Supplementary Figs. 3f and 4b). Altogether, this indicates that OTUD5 is not required for NHEJ in a general, nonspecific chromatin context, but promotes end-joining mediated DNA repair pathways (both NHEJ and MMEJ), in a context-specific manner, at telomeres.

OTUD5 promotes ATM-dependent DDR activation by regulating the UBR5-ATMIN axis

After establishing a role for OTUD5 in promoting ATM-dependent DDR and DNA repair at deprotected telomeres, we sought to further understand the underlying regulatory circuit. OTUD5 was previously reported to play a role in transcriptional repression at damaged chromatin by stabilizing the E3 ubiquitin ligase UBR5[25]. Independently, UBR5 has been reported to promote ATM activation by inhibiting ATMIN, a negative regulator of DSB-induced ATM activity, through non-degradative ubiquitination[26]. These previously established links prompted us to hypothesize that OTUD5 promotes ATM-dependent DDR and telomeric DNA repair in a UBR5 and ATMIN-dependent manner. To test our hypothesis, we first assessed whether there is any detectable interaction between OTUD5, UBR5, ATMIN and ATM. We ectopically expressed GFP-tagged OTUD5 in HEK293T cells and performed co-immunoprecipitation. Despite our expectation that OTUD5 interacts directly only with UBR5 and interacts transiently and indirectly with ATMIN and/or ATM, thereby posing a challenge for detection, we readily detected an interaction of OTUD5 with all three endogenous proteins (UBR5, ATMIN and ATM) (Fig. 4a).

Next, we assessed the potential functional involvement of UBR5 in OTUD5-promoted KAP1^{S824} phosphorylation, by depleting OTUD5, UBR5, or both in U2OS cells. In line with previous findings in the context of transcriptional repression, depletion of OTUD5 led to reduced levels of endogenous UBR5 protein, both in the absence and presence of IR (Fig. 4b). Upon IR, U2OS cells lacking either OTUD5 or UBR5 displayed reduced pKAP1^{S824} (Fig. 4b), revealing that not only OTUD5, but also UBR5 is important for efficient KAP1^{S824} phosphorylation upon DNA damage. Furthermore, depletion of OTUD5 in UBR5-deficient cells did not further aggravate the pKAP1^{S824} defect of these cells, indicating that OTUD5 and UBR5 act in an epistatic manner to promote KAP1^{S824} phosphorylation, by OTUD5 acting upstream of UBR5 to stabilize it. In further support of this, depletion of UBR5 with independent sgRNAs in TRF2ts MEFs recapitulated the KAP1^{S824} phosphorylation defect displayed by OTUD5-depleted TRF2ts MEFs (Fig. 4c). Moreover, loss of UBR5 also significantly reduced telomere fusions upon telomere deprotection (Fig. 4d, e, Supplementary Fig. 5a). Of note, we observed that protein abundance of OTUD5 is elevated in UBR5-deficient cells (Fig. 4b, c). This could indicate some

https://doi.org/10.1038/s41467-024-53404-0

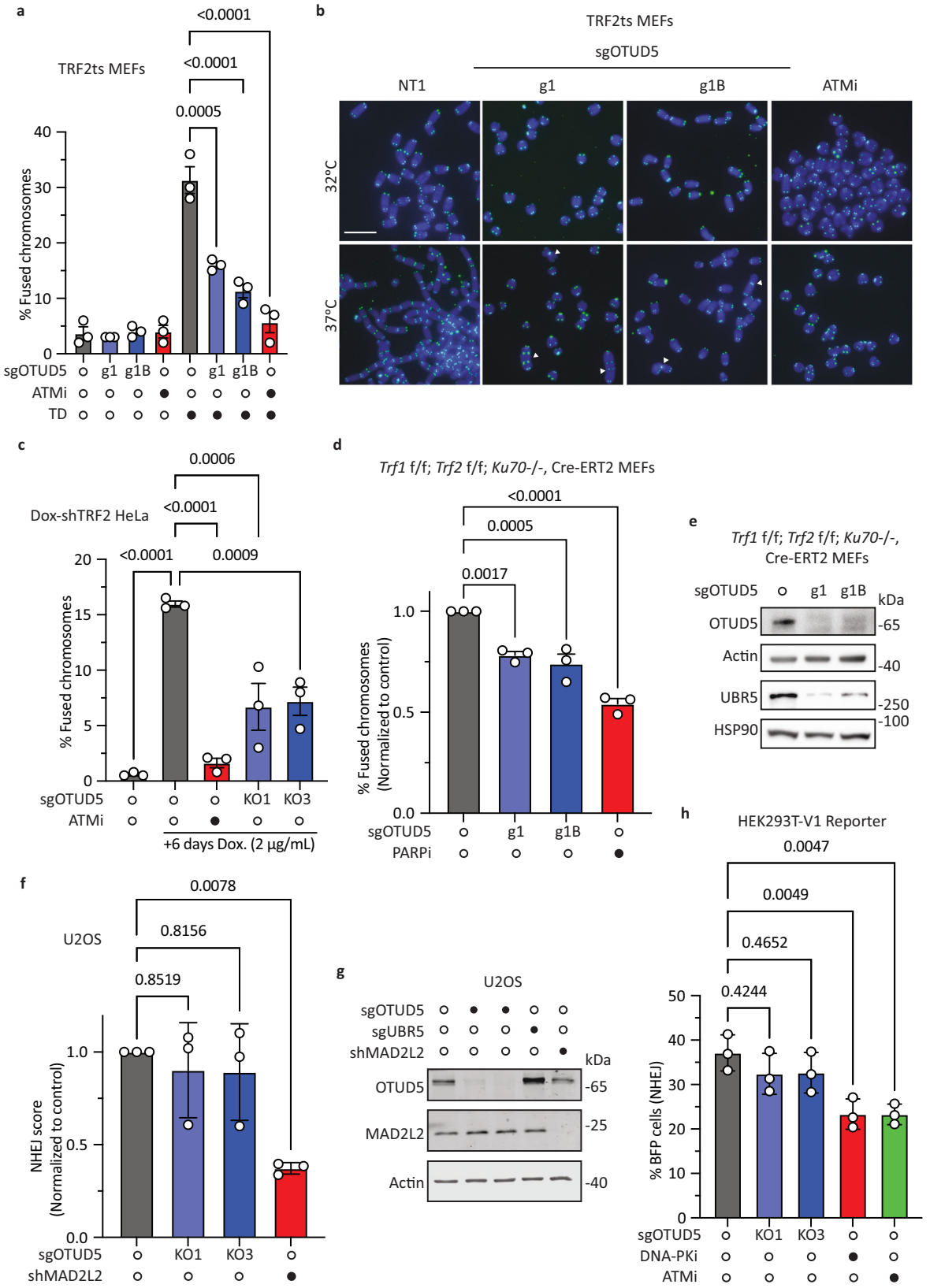

form of internal homeostasis in ubiquitination-mediated regulation of protein stability between OTUD5 and UBR5.

UBR5 is known to promote DSB-induced DDR by counteracting ATMIN-mediated inhibition on ATM[26]. If OTUD5 indeed promotes ATM-dependent DDR and telomeric DNA repair through the UBR5-ATMIN axis, ablation of ATMIN is expected to reverse the DDR defects exhibited by OTUD5-depleted cells. To test this, we inhibited ATMIN expression in OTUD5-depleted TRF2ts MEFs by using 3 independent shRNAs (#5, #24, #84) (Supplementary Fig. 5b). In line with our hypothesis, depletion of ATMIN strongly and significantly rescued both the KAP1^{S824} phosphorylation defect and the telomere fusion defect of OTUD5-depleted cells (Fig. 4f, g, Supplementary Fig. 5c).

Fig. 3 | OTUD5 promotes NHEJ and MMEJ preferentially at telomeres. **a** Quantification of chromosome end-to-end fusions in control (sgNT1) and OTUD5-depleted (sgOTUD5 g1/g1B) TRF2ts MEFs with (37 °C, 36 h) or without (32 °C) telomere deprotection. For ATM inhibition (ATMi), cells were pretreated with 10 μM KU-55933 1 h before telomere deprotection. Bars represent means ± SEM. Each dot represents one of three independent experiments. Statistical analysis: one-way ANOVA with Dunnett's multiple comparisons test. **b** Representative images from one of three independent replicates in (**a**). Scale bar represents 10 μm. **c** Quantification of chromosome fusions in control (sgNT1) and OTUD5-depleted (sgOTUD5 KO1/KO3) HeLa doxycycline-inducible shTRF2 cells with (6 days doxycycline, 2 μg/mL) or without (no doxycycline) telomere deprotection. For ATM inhibition (ATMi), cells were pretreated with 10 μM KU-55933 1 h before telomere deprotection. Bars represent means ± SEM. Each dot represents one of three independent experiments. Statistical analysis was performed according to one-way ANOVA with Dunnett's multiple comparisons test between samples. **d** Assessment of chromosome fusions upon Cre-mediated TRF1 and TRF2 loss in OTUD5-depleted (sgOTUD5 g1/g1B) *Trf1*$^{f/f}$;*Trf2*$^{f/f}$;*Ku70*$^{-/-}$;Cre-ERT2 MEFs treated with 0.5 μM 4-hydroxytamoxifen (4-OHT) for 108 h. For PARP inhibition (PARPi), cells were treated with 0.5 μM Olaparib 60 h before harvesting. The % fused chromosomes in each sample is normalized to control (sgNT1). Bars represent means ± SEM. Each dot represents one of three independent experiments. Statistical analysis: one-way ANOVA with Dunnett's multiple comparisons test. **e** Immunoblot analysis of OTUD5 and UBR5 in *Trf1*$^{f/f}$;*Trf2*$^{f/f}$;*Ku70*$^{-/-}$;Cre-ERT2 MEFs used in (**d**). Actin and HSP90 serve as loading controls for OTUD5 and UBR5 respectively. Representative blot from three independent experiments. **f** Assessment of NHEJ efficiency by random plasmid integration in control (sgNT1), OTUD5-depleted (sgOTUD5 KO1/KO3) and MAD2L2-depleted (shMAD2L2) U2OS cells. NHEJ scores in each sample are normalized to control (sgNT1). Bars represent means ± SEM. Each dot represents one of three independent experiments. Statistical analysis: one-way ANOVA with Dunnett's multiple comparisons test. **g** Immunoblot analysis for OTUD5 and MAD2L2 in U2OS cells used in (**f**). Actin serves as loading control. Representative blot from three independent experiments**. h** Assessment of NHEJ efficiency (% BFP) in control (sgNT1), OTUD5-depleted (sgOTUD5 KO3), DNAPKi-treated (10 μM KU-57788) and ATMi-treated (10 μM KU-55933) DSB-Spectrum_V1 reporter HEK293T cells. Bars represent means ± SEM. Each dot represents one of three independent experiments. Statistical analysis: one-way ANOVA with Dunnett's multiple comparisons test. Source data are provided as a Source Data file.

Furthermore, depletion of OTUD5 did not further aggravate the telomere fusion defect of ATM inhibitor-treated cells (Fig. 4h, Supplementary Fig. 5d). Taken together, these results indicate that the functional role of OTUD5 in DDR activation and end-joining at dysfunctional telomeres relies on its control of the UBR5-ATMIN-ATM regulatory axis.

OTUD5 promotes telomeric end-joining by promoting KAP1^{S824} phosphorylation

To further investigate the mechanism underlying the control of end-joining mediated repair by OTUD5, we first considered the possibility that OTUD5 (in part) facilitates telomeric NHEJ by promoting the stability of the core NHEJ factor Ku80. This, since it has been reported that OTUD5 counteracts proteasomal degradation of Ku80 in certain cell lines[39]. To address this, we assessed the protein levels of Ku80 in OTUD5-depleted TRF2ts MEFs and U2OS cells. However, contrary to the previously reported finding in different cell lines, loss of OTUD5 did not lead to a reduction in Ku80 protein levels in MEFs or U2OS cells, regardless of DNA damage induction by IR or telomere deprotection (Supplementary Fig. 6a, b). Thus, OTUD5 does not appear as a critical regulator of Ku stability in the cell types of our study, in line with that multiple E3s and DUBs have been implicated in controlling Ku stability[39,40]. Moreover, destabilization of Ku80 is also unlikely to explain the telomere end-joining defects in OTUD5-depleted cells, as OTUD5-depleted cells also display reduced telomere MMEJ in cells deficient for TRF1, TRF2 and Ku70, where Ku80 is both dispensable and absent. Additionally, destabilization of a pivotal NHEJ factor such as Ku80 would impair global NHEJ significantly, regardless of genomic context, which is not what we observed for OTUD5-deficient cells. Hence, we conclude that the impact of OTUD5 on telomeric end-joining in the cells and conditions of our assays, is not mediated via changes in the level of Ku70/80.

At deprotected telomeres, ATM-dependent recruitment of 53BP1 is a critical determinant of NHEJ efficiency[41]. As OTUD5-depleted cells display impaired ATM activation and ATM-dependent DDR, it reasonably follows that 53BP1 recruitment could be compromised in these cells, giving rise to defective telomere NHEJ. To address this, we measured co-localization of 53BP1 foci with telomeres by IF-FISH upon TRF2 inactivation in TRF2ts cells. While treatment with an ATM inhibitor completely abolished the appearance of 53BP1 telomere dysfunction induced foci (TIFs), OTUD5 depletion did not hinder 53BP1 accumulation at deprotected telomeres (Fig. 5a, Supplementary Fig. 6d). This indicates that the residual ATM activity in OTUD5-depleted cells is sufficient to support efficient 53BP1 recruitment to dysfunctional telomeres, and that the telomere end-joining defect in OTUD5-depleted cells is not caused by failed 53BP1 recruitment.

We next assessed the recruitment of RIF1 in response to telomere deprotection in OTUD5-depleted cells, by immunofluorescence. RIF1 is a key NHEJ factor that is recruited to DSBs and dysfunctional telomeres in an ATM and 53BP1-dependent manner and promotes end-joining by restricting DNA end resection[42–45]. In line with previous findings, ATM inhibitor treatment fully abolished RIF1 foci formation upon telomere deprotection. On the other hand, RIF1 foci formation was only mildly impaired in OTUD5-depleted cells, reaching statistical significance for only one of the two sgRNAs (sgOTUD5 g1B) used (Fig. 5b, Supplementary Fig. 6e), thereby recapitulating only a fraction of the effect of ATM inhibitor treatment. Similar to RIF1 foci, formation of γH2A.X foci upon telomere deprotection was marginally compromised in cells treated with sgOTUD5 g1B and not significantly changed with the other sgRNA (Supplementary Fig. 6c, f).

Despite that ATM activity was not compromised to an extent that abolishes 53BP1 and RIF1 recruitment, the impairment in ATM-dependent DDR signaling, especially that of KAP1^{S824} phosphorylation, is substantial. Hence, we next considered the possibility that KAP1, the central factor of our screening approach, is itself of key importance for how OTUD5 promotes efficient DNA repair activity at telomeres. KAP1 is known to be a heterochromatin scaffold protein that orchestrates the formation and maintenance of heterochromatin[46,47]. At heterochromatic DSBs, KAP1 imposes a strong hindrance on DNA repair by maintenance of a compact, non-permissive chromatin state that deters DNA repair factors[17–19,48]. ATM-dependent phosphorylation of KAP1 is essential to potentiate local chromatin decompaction to enable DNA repair, and ectopic overexpression of a KAP1^{S824D} phosphomimic mutant is able to fully restore DNA repair efficiency at heterochromatic DSBs that is crippled by ATM dysfunction. Although telomeres are not entirely heterochromatic by consent[49,50], they are enriched in heterochromatin-binding factors KAP1 and HP1 in both mouse and human cells[51–53], and telomere deprotection strongly triggers KAP1^{S824} phosphorylation.

To address the significance of KAP1 in telomere NHEJ, we first individually, or in combination, depleted KAP1 and OTUD5 in TRF2ts MEFs and assessed telomere fusions upon telomere deprotection. Strikingly, not only did depletion of KAP1 drastically enhance telomere fusions, but it also completely abolished the telomere fusion defect of OTUD5-deficient cells, indicating that OTUD5 facilitates telomeric NHEJ in a KAP1-dependent manner (Fig. 5c, d, Supplementary Fig. 7a). To address the functional significance of KAP1^{S824} phosphorylation at deprotected telomeres, we ectopically expressed the phosphomimic KAP1^{S824D} mutant and assessed if this rescues the telomeric NHEJ defect

https://doi.org/10.1038/s41467-024-53404-0

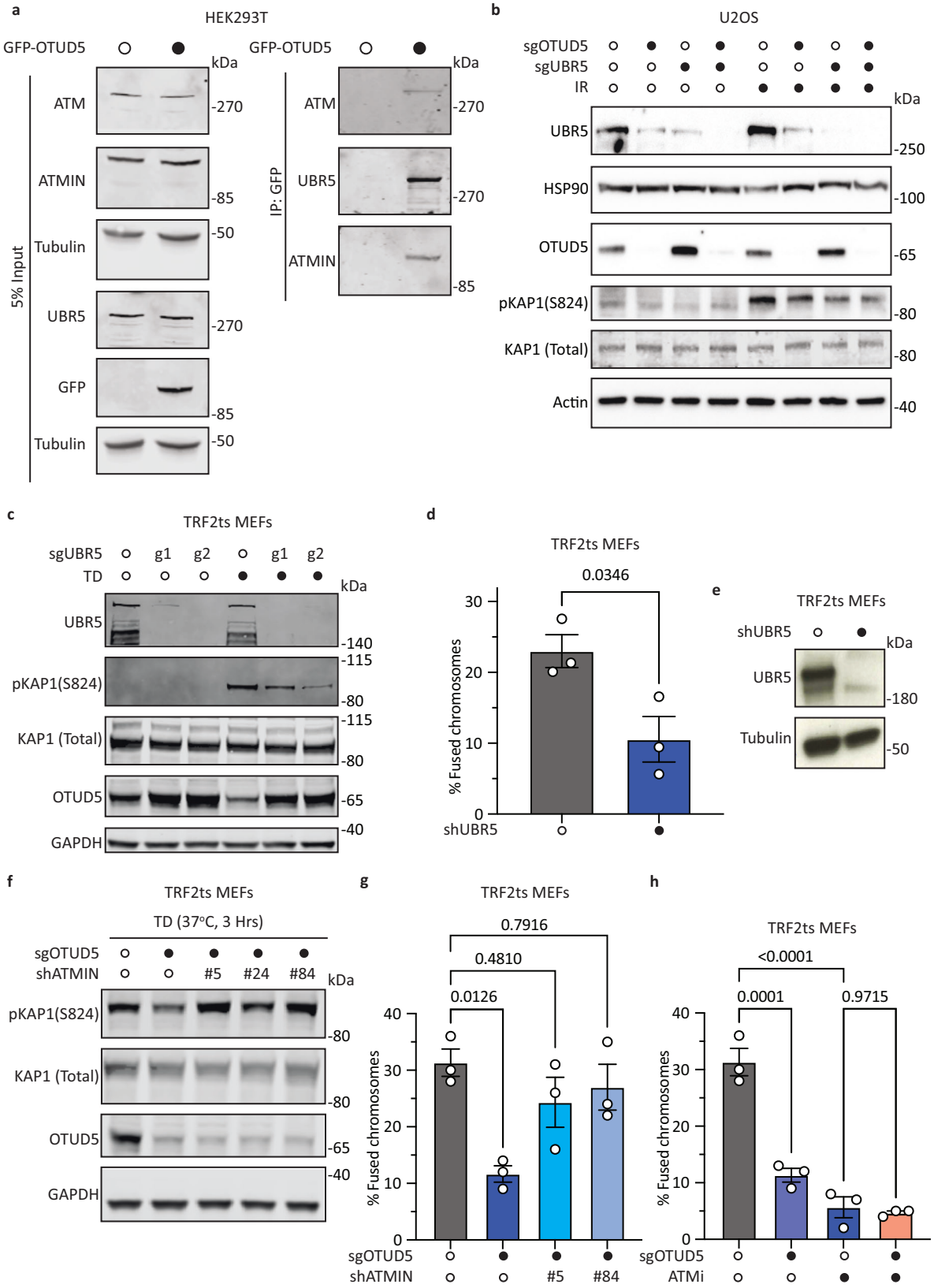

of OTUD5-depleted cells. Indeed, overexpression of KAP1^{S824D} restored telomere fusion efficiency in OTUD5-depleted cells, while ectopic expression of wild-type (KAP1^{WT}) failed to do so (Fig. 5e, f, Supplementary Fig. 7b, c). From this, we conclude that KAP1 and KAP1^{S824} phosphorylation play a prominent role in telomere NHEJ, and that OTUD5 facilitates telomere NHEJ by promoting ATM-dependent KAP1^{S824} phosphorylation. Moreover, ectopic expression of phosphomimic KAP1^{S824D} also rescued the telomere MMEJ defect in OTUD5-depleted *Trf1$^{F/F}$;Trf2$^{F/F}$;Ku70$^{-/-}$;p53$^{-/-}$;Cre-ER^{T2}* MEFs (Fig. 5g, Supplementary Fig. 7d, e). Together, these results indicate that the phosphorylation status of KAP1^{S824} is an important functional determinant for end-joining efficiency (both NHEJ and MMEJ) at dysfunctional

Fig. 4 | OTUD5-dependent promotion of KAP1^{S824} phosphorylation and telomere NHEJ are epistatic with the UBR5-ATMIN axis. a Immunoblot analysis of ATM, ATMIN, and UBR5 levels upon immunoprecipitation of GFP-OTUD5 in HEK293T cells. Tubulin serves as loading control. Representative blot from three independent experiments. **b** Immunoblot analysis of pKAP1^{S824} levels in OTUD5-depleted (sgOTUD5 KO1), UBR5-depleted (sgUBR5 KO1), OTUD5/UBR5 double-depleted and control (sgNT1) U2OS cells, untreated or treated with ionizing radiation (IR; 3 Gy, 30 min recovery at 37 °C). Actin serves as loading control for KAP1 and OTUD5. HSP90 serves as loading control for UBR5. Representative blots from three independent experiments. **c** Immunoblot analysis of pKAP1^{S824} levels in UBR5-depleted (sgUBR5 g1/g2) and control (sgNT1) TRF2ts MEFs with (37 °C, 3 h) or without (32 °C) telomere deprotection. GAPDH serves as loading control. Representative blots from three independent experiments. **d** Quantification of chromosome fusions in control (shScramble) and UBR5-depleted (shUBR5) TRF2ts MEFs, with (37 °C, 36 h) telomere deprotection. Bars represent means ± SEM. Each dot represents one of three independent experiments. Statistical analysis was performed according to unpaired two-tailed Student's t-test between samples as indicated. **e** Immunoblot validation of UBR5 depletion (shUBR5) in TRF2ts MEFs used in (**d**). Tubulin serves as loading control. Representative blot from three independent experiments. **f** Immunoblot analysis of pKAP1^{S824}, KAP1 and OTUD5 in control TRF2ts MEFs (sgNT1) and OTUD5-depleted TRF2ts MEFs (sgOTUD5 g1b) with or without ATMIN depletion (shATMIN #5/#24/#84) and subjected to telomere deprotection. GAPDH serves as loading control. Representative blots from three independent experiments. **g** Quantification of chromosome fusions in control (sgNT1) and OTUD5-depleted (sgOTUD5 g1b) TRF2ts MEFs with or without ATMIN depletion (shATMIN #5/#84) and subjected to telomere deprotection (37 °C, 36 h). Bars represent means ± SEM. Each dot represents one of three independent experiments. Statistical analysis: one-way ANOVA with Dunnett's multiple comparisons test. **h** Quantification of chromosome fusions in control (sgNT1), OTUD5-depleted (sgOTUD5 g1b) TRF2ts MEFs with (37 °C, 36 h) or without (32 °C) telomere deprotection. For ATM inhibition, cells were pretreated with 10 μM KU-55933 30 min before telomere deprotection. Bars represent means ± SEM. Each dot represents one of three independent experiments. Statistical analysis: one-way ANOVA with Dunnett's multiple comparisons test. Source data are provided as a Source Data file.

telomeres and is the critical node through which OTUD5 facilitates telomeric DNA repair.

It has been reported that at DSBs in heterochromatic regions, where KAP1 is enriched, the phosphorylation of KAP1 promotes DNA repair by facilitating the displacement of the nucleosome remodeler CHD3, thereby triggering transient chromatin decompaction[19]. To test whether KAP1 phosphorylation promotes telomeric DNA repair in a similar manner as it does at DSBs in heterochromatin, we quantified telomere fusions at deprotected telomeres in TRF2ts MEFs depleted of CHD3. However, unlike ablation of KAP1, we did not observe an increase in telomere fusions in the absence of CHD3 (Supplementary Fig. 8a, b). Besides indicating that CHD3 is irrelevant to NHEJ of TRF2-deprotected telomeres, this suggests either that KAP1 functions via a different, potentially redundant, chromatin remodeler at telomeres, or that the phosphorylation of KAP1 promotes NHEJ at telomeres through a mechanism independent of CHD3 or chromatin decompaction.

OTUD5 is required for the efficient repair of IR-induced DNA damage in heterochromatin

Given the role of OTUD5 in DNA repair at dysfunctional telomeres by promoting ATM-dependent KAP1^{S824} phosphorylation, and the established importance of KAP1^{S824} phosphorylation for repair of heterochromatic DSBs[17–19,48], we investigated whether OTUD5 also facilitates DSB repair at heterochromatin. Hereto we tracked the rate of resolution of IR-induced γH2A.X foci associated with heterochromatic chromocenters in NIH3T3 cells[17]. After induction of DSBs by IR, over 90% of induced γH2A.X foci associated with chromocenters were resolved within 24 h (Fig. 6a–d, Supplementary Fig. 8c). In contrast, and as demonstrated before[17], cells pre-treated with ATM inhibitor were inefficient in resolving heterochromatin-associated γH2A.X foci, retaining 70% of induced foci after 24 h of recovery. OTUD5-depleted cells also showed reduced resolution of γH2A.X foci, with ~40% of heterochromatin-associated foci remaining unresolved at 24 h after IR, indicating inefficient repair of DSBs at heterochromatic regions. Thus, in addition to telomeres, OTUD5 also plays a role in facilitating DNA repair at heterochromatic regions, in line with the here uncovered role of OTUD5 in regulating KAP1.

Discussion

Ubiquitin system factors play a major role in orchestrating responses to DNA damage[20]. The DUB OTUD5 was previously shown to suppress transcription at DNA breaks[25]. Using a novel screening approach, we now revealed OTUD5 as a prominent promotor of ATM activation and ATM-dependent KAP1 phosphorylation, in response to both telomere deprotection and genome-wide DSBs. Moreover, we found that OTUD5 promotes DNA repair at deprotected telomeres and at heterochromatin. The role of OTUD5 in transcriptional suppression has been ascribed to its ability to stabilize UBR5. Indeed, we confirm destabilization of UBR5 upon loss of OTUD5. As independently, UBR5 was found to inhibit the interaction between ATM and ATMIN, a negative regulator of canonical DSB-induced ATM activation[26], we hypothesized that OTUD5 may promote ATM-dependent DDR signaling via stabilization of UBR5. Indeed, we found OTUD5 to promote ATM-dependent DDR signaling in a manner that is epistatic with UBR5, dependent on its catalytic activity and involving ATMIN, supporting that OTUD5 acts via UBR5.

Early biochemical studies performed on OTUD5 suggested that phosphorylation at residue Ser-177 is vital for its DUB activity in vitro[24]. Consistent with this, we showed that the phospho-activation of OTUD5 is indispensable to its function in promoting DDR signaling, as phospho-dead OTUD5^{S177A} failed to restore the pKAP1^{S824} level in OTUD5-depleted cells. This demonstrates the biological significance of phospho-regulation to the functions of OTUD5 in vivo. To date, little is known about the kinases that phosphorylate OTUD5, apart from recent in vivo evidence that mTOR kinase promotes OTUD5 stability and activity via direct phosphorylation of multiple sites on OTUD5. This in turns activates mTORC1/2, thereby constituting positive feedback signaling[54,55]. It is conceivable that also in the DDR, an upstream kinase phosphorylates OTUD5 to amplify DDR signaling through a similar positive feedback mechanism. Of note, OTUD5 contains multiple conserved SQ sites (S425, S497, S549) roughly within an SCD domain (≥3 S/TQ sites within 100 amino acids), which are features of ATM/ATR kinase substrates[56,57]. This suggests the possibility that OTUD5 is directly phosphorylated by ATM to function as an amplifier of ATM-dependent DDR signaling in a potential positive-feedback circuit, resembling its role in mTOR signaling.

In the context of DNA repair, OTUD5 has been suggested to promote NHEJ by counteracting the degradation of Ku80, a core NHEJ factor, in certain cell lines[39]. Contrary to that work, we find in MEFs and U2OS cells that Ku80 stability is not compromised in the absence of OTUD5. This indicates that in these cells OTUD5 is not a critical regulator of Ku stability and that other DUBs, such as potentially UCHL3, are dominantly responsible for stabilizing Ku[40]. In line with this, we did not observe a significant defect in genome-wide NHEJ in OTUD5-depleted cells, which would be expected from Ku70/80-deficient cells. Instead, we propose that OTUD5 facilitates DNA repair exclusively in genomic regions that are particularly sensitive to ATM activity, such as telomeres and heterochromatin[5,17], by promoting full DDR-induced ATM activity via the UBR5-ATMIN axis.

Despite impaired ATM activation, recruitment of 53BP1 (and most of RIF1) to deprotected telomeres, an ATM-dependent process[5], is unaffected in OTUD5-depleted cells. We reason that the loss of OTUD5

https://doi.org/10.1038/s41467-024-53404-0

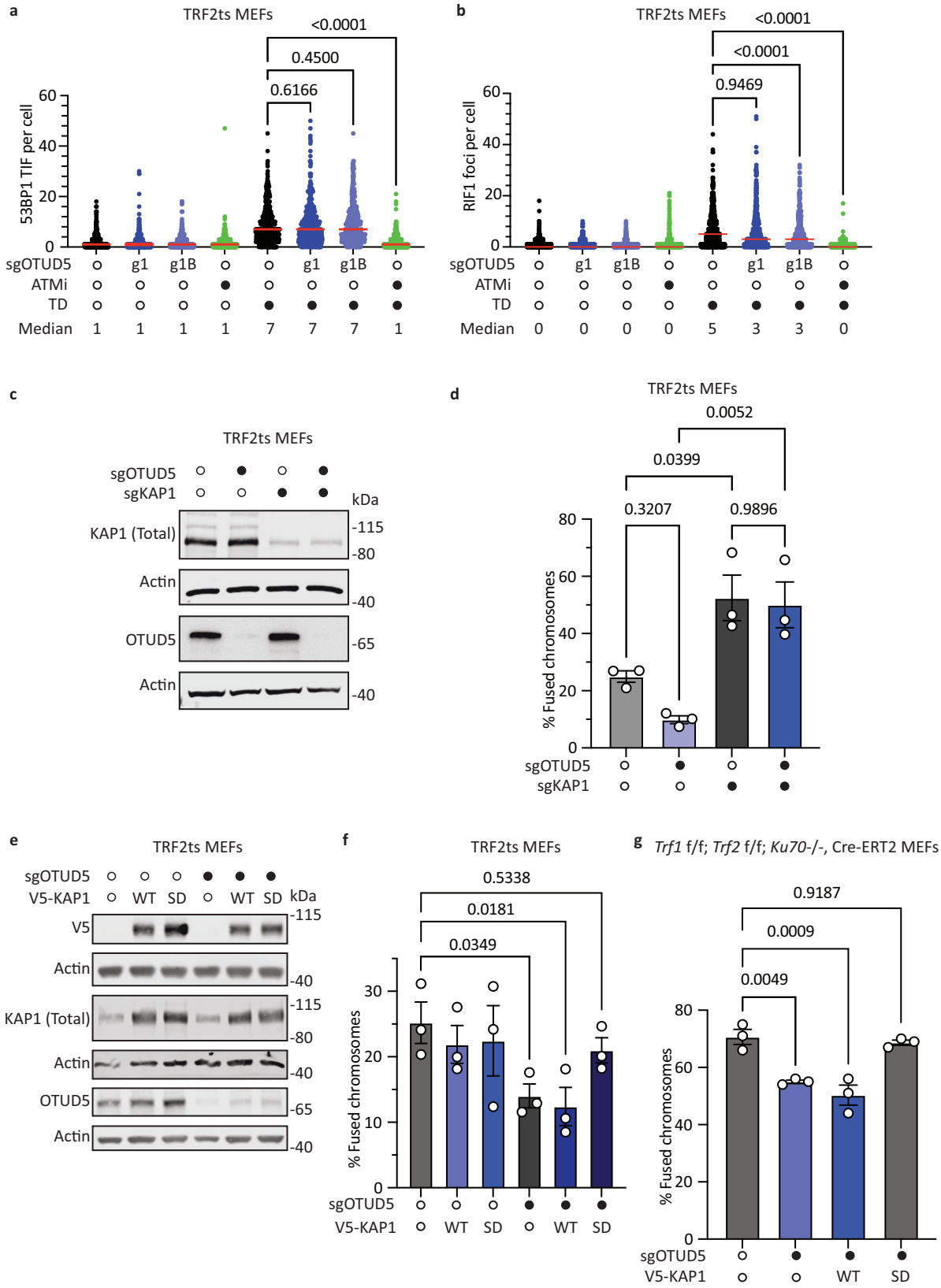

is insufficient to abolish all aspects of ATM function, and that the residual ATM activity is sufficient to support 53BP1 (and RIF1) recruitment. This indicates also that the cause of the end-joining defect in OTUD5-deficient cells lies downstream of the end-joining promoting activity of 53BP1. We demonstrate here that this is at the level of KAP1. We show that pKAP1^{S824}, amongst other ATM targets, is an especially sensitive and functionally important substrate that dictates NHEJ efficiency at telomeres. The sensitivity of KAP1 phosphorylation to disturbance in ATM activity is in line with previous observations stating that KAP1 phosphorylation requires localized, concentrated ATM activity[18], which may not be achieved in OTUD5-deficient cells. This localized, concentrated ATM activity has been ascribed to hyper-

Fig. 5 | OTUD5 promotes end-joining at deprotected telomeres in a KAP1 and pKAP1^{S824}-dependent manner. Quantification of average 53BP1 (**a**) or RIF1 (**b**) telomere dysfunction-induced foci (TIFs) per cell in OTUD5-depleted TRF2ts MEFs (sgOTUD5 g1/g1B), untreated or treated with telomere deprotection (37 °C, 3 h), compared to control (sgNT1) and ATM inhibitor (10 μM KU-55933)-treated cells. For ATM inhibition, cells were pretreated with 10 μM KU-55933 30 min before telomere deprotection. Statistical analysis was performed according to one-way ANOVA with Dunnett's multiple comparisons test. Each dot represents a data point from three independent experiments. Assessment of telomere fusions in OTUD5-depleted TRF2ts MEFs (sgOTUD5 g1B) with or without KAP1 depletion. **c** Immunoblot validation of KAP1 and OTUD5 depletion in TRF2ts MEFs used in (**d**). Actin serves as loading control. Representative blots from three independent experiments. **d** Quantification of chromosome fusions in control (sgNT1), OTUD5-depleted, KAP1-depleted, and OTUD5-KAP1 double depleted TRF2ts MEFs upon telomere deprotection at 37 °C for 36 h. Bars represent means ± SEM. Each dot represents one of three independent experiments. Statistical analysis was performed according to unpaired two-tailed Student's t-test between paired samples as indicated. **e**, **f** Assessment of telomere fusions in OTUD5-depleted TRF2ts MEFs (sgOTUD5 g1B) with or without complementation of pLX304-V5-KAP1 (wildtype (WT) or S824D). **e** Immunoblot validation of OTUD5 depletion and V5-KAP1 (wildtype (WT) or S824D) overexpression in TRF2ts MEFs used in (**f**). Actin serves as loading control. Representative blots from three independent experiments. **f** Quantification of chromosome fusions in control (sgNT1), OTUD5-depleted (sgOTUD5 g1b) TRF2ts MEFs with or without complementary expression of V5-KAP1 (wildtype (WT) or S824D (SD)) upon telomere deprotection at 37 °C for 36 h. Bars represent means ± SEM. Each dot represents one of three independent experiments. Statistical analysis was performed according to one-way ANOVA with Dunnett's multiple comparisons test. **g** Quantification of chromosome fusions in control (sgNT1), OTUD5-depleted (sgOTUD5 g1b) *Trf1*$^{f/f}$;*Trf2*$^{f/f}$;*Ku70*$^{-/-}$;Cre-ERT2 MEFs with or without complementary expression of V5-KAP1 (wildtype (WT) or S824D (SD)) upon telomere deprotection by treatment with 0.5 μM 4-OHT for 108 h. Bars represent means ± SEM. Each dot represents one of three independent experiments. Statistical analysis was performed according to one-way ANOVA with Dunnett's multiple comparisons test between samples. Source data are provided as a Source Data file.

accumulation of the MRN complex, mediated via the C-terminal BRCT-domain of 53BP1[18]. Although 53BP1 recruitment seemed unperturbed, the reduced RIF1 foci in one of the OTUD5 KO cell lines suggest incomplete phosphorylation of the 53BP1 N-terminus. It remains possible that incomplete ATM-dependent 53BP1 phosphorylation contributes to the reduced KAP1 phosphorylation in OTUD5 deficient cells. Furthermore, telomere deprotection via TRF2 loss/inactivation strictly triggers ATM activation as ATR activation remains inhibited via shelterin factor POT1[5]. This precludes phosphorylation of ATM substrates via the ATR kinase, which has been shown to compensate for loss of ATM in global NHEJ[58]. This lack of compensatory KAP1 phosphorylation via ATR adds to the exquisite sensitivity of telomeric NHEJ to disturbances in ATM activation. The need for robust KAP1 phosphorylation at deprotected telomeres is evident in the impaired end-joining observed in OTUD5-deficient cells, where KAP1 phosphorylation is lacking and end-joining at deprotected telomeres is restored upon ectopic overexpression of phosphomimic KAP1.

The significance of KAP1^{S824} phosphorylation in telomeric DNA repair shares similarities with its previously reported function in DNA repair at heterochromatin[16,17]. Different from euchromatin, a substantial challenge for DNA repair at heterochromatin is its compact, sterically non-permissive conformation. Without chromatin relaxation, it is difficult to repair DNA lesions at heterochromatin, as access of DNA repair factors is restricted. Among ATM substrates, KAP1 is central to heterochromatic DNA repair as KAP1^{S824} phosphorylation is necessary for the eviction of CHD3 and other heterochromatin factors from heterochromatin to achieve a relaxed conformation that is beneficial to DNA repair[19]. Ablation of KAP1 or CHD3, or complementation with a phosphomimic KAP1^{S824D}, is sufficient to bypass the requirement of ATM, demonstrating a pivotal function for KAP1^{S824} phosphorylation in facilitating heterochromatic DNA repair, by promoting local chromatin decompaction. Our data here reveal that DNA repair at telomeres phenotypically resembles that of heterochromatin *prima facie*, in the sense that KAP1^{S824} phosphorylation is required for efficient DNA repair in both genomic contexts. However, intriguingly, it has been reported that deprotected telomeres do not require, nor undergo, chromatin decompaction for DNA repair to take place[59,60], suggesting that KAP1^{S824} phosphorylation is unlikely to promote telomere end-joining through decompaction of telomeric chromatin. In line with this notion, contrary to KAP1 depletion, loss of CHD3 did not elevate telomere fusion. This indicates that despite the mutual requirement of ample KAP1 phosphorylation for DNA repair at heterochromatin and deprotected telomeres, the underlying mechanism is likely different for the two genomic contexts. Thus, the mechanism underlying the requirement of KAP1 phosphorylation at deprotected telomeres, is not immediately clear and requires further exploration in future studies.

One interesting possibility to investigate relates to the ability of both KAP1 and shelterin components TRF1 and TRF2 to interact with nuclear lamina components[61–64]. The interaction of KAP1 with nuclear lamina components has been postulated to contribute to the transcriptional silencing of KAP1-associated heterochromatin, by tethering heterochromatin to the nuclear lamina[62,65]. In a similar fashion, KAP1 may tether telomeric DNA to the nuclear lamina, in a way, involving transcriptional control or not, that negatively impacts telomeric DNA repair and is modulated by KAP1^{S824} phosphorylation. In addition, the role of KAP1 in transcriptional silencing may also independently from nuclear lamina interactions affect DNA repair, given the increasing implications of RNA in DNA repair[66]. Alternatively, it is possible that KAP1 phosphorylation serves to promote mobility of the damaged ends, as both deprotected telomeres and heterochromatic DSBs have been shown to have an increased mobility within the nucleus. This increased mobility has been proposed to increase the chance of two free DNA ends reconnecting[41,67].

In addition to the facilitation of telomeric DNA repair by KAP1^{S824} phosphorylation, our data also indicates an unexpected protective role of KAP1 at dysfunctional telomeres by inhibiting NHEJ, as direct ablation of KAP1 considerably increased the frequency of telomere fusion in the absence of TRF2 function. KAP1 and HP1 are heterochromatin scaffold proteins that are enriched at heterochromatic regions and serve as a recruitment hub for histone methyltransferases, deacetylases, and chromatin remodelers that act in orchestration to promote the formation and maintenance of heterochromatic chromatin state. Despite the knowledge that KAP1 and HP1 are enriched in the telomeric proteome in both human and mouse cells[51,53], little is known about their functional roles at telomeres. Intriguingly, human telomeres were reported to not be enriched in heterochromatic histone signatures like H3K9me3 or H3K27me3[49]. Thus, it is enigmatic why these heterochromatin factors are present despite that there is no heterochromatin to maintain. Our data on KAP1 implies the involvement of heterochromatin factors in the maintenance and protection of telomeres against unwarranted DNA repair. This provides a plausible functional explanation for the presence of heterochromatin factors at telomeres. It is worth exploring through what mechanisms KAP1, and potentially HP1, inhibit telomeric DNA repair, especially since KAP1 is frequently upregulated in cancers, with correlation to enhanced invasiveness and poor survival in patients[68–70]. Further understanding on the link between KAP1 and telomeres may potentiate advancement of our understanding on telomere biology in cancers.

Altogether, our work identifies an important role for OTUD5 in promoting DDR and particularly KAP1^{S824} phosphorylation through an OTUD5-UBR5-ATMIN-ATM axis. Loss of OTUD5 confers a DNA repair

https://doi.org/10.1038/s41467-024-53404-0

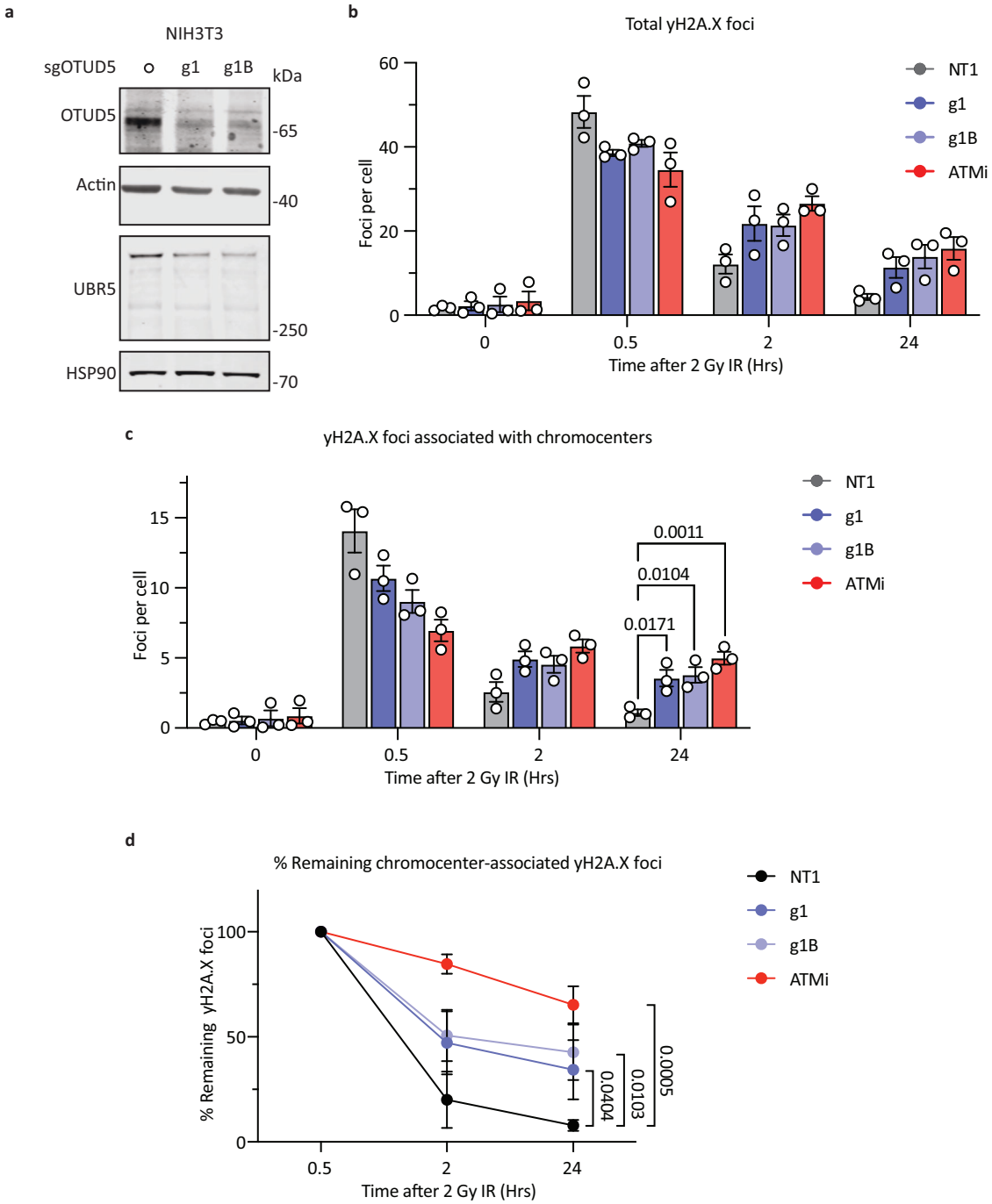

Fig. 6 | OTUD5 promotes DNA repair at heterochromatin. a Immunoblot validation of OTUD5 depletion (sgOTUD5 g1/g1B) in NIH3T3 cells used in (**b**–**d**). Actin serves as loading control. **b**–**d** Assessment of rates of resolution of IR-induced γH2A.X foci (total/chromocenter-associated) in OTUD5-depleted NIH3T3. **b** Quantification of total γH2A.X foci in control (sgNT1), OTUD5-depleted (sgOTUD5 g1/g1B) and ATM inhibitor-treated (ATMi, KU-55933, 10 μM, treated 30 min before IR) cells at 0 (untreated), 0.5, 2, 24 h after IR (2 Gy). Bars represent means ± SEM. Each dot represents one of three independent experiments. **c** Quantification of chromocenter-associated γH2A.X foci in control (sgNT1), OTUD5-depleted (sgOTUD5 g1/g1B) and ATM inhibitor-treated (ATMi; 10 μM KU-55933) cells at 0 (untreated), 0.5, 2, 24 h after IR (2 Gy). Bars represent means ± SEM. Each dot represents one of three independent experiments. Statistical analysis was performed according to two-way ANOVA with Dunnett's multiple comparisons test. **d** Quantification of the percentage of chromocenter-associated γH2A.X foci remaining in control (sgNT1), OTUD5-depleted (sgOTUD5 g1/g1B) and ATM inhibitor-treated (ATMi; 10 μM KU-55933) cells at 0.5, 2, 24 h after IR (2 Gy), individually normalized to the respective amount of chromocenter-associated γH2A.X foci at 0.5 h after IR (2 Gy). Bars represent means ± SEM. Statistical analysis was performed according to two-way ANOVA with Dunnett's multiple comparisons test. Source data are provided as a Source Data file.

defect most prevalent in regions enriched in KAP1, both at deprotected telomeres and heterochromatic DSBs. In addition, our work points at an unanticipated role of KAP1 in suppressing toxic end-joining activity at dysfunctional telomeres, the mechanistic basis of which is interesting to explore in future studies.

Methods

Cell Culture

HEK293T, U2OS and NIH3T3 cells were obtained from ATCC. *Trf2*$^{-/-}$;*p53*$^{-/-}$;TRF2ts MEFs (TRF2ts MEFs) were generated from *Trf2*$^{flox/-}$;*p53*$^{-/-}$ MEFs as previously described[71]. *Trf2*$^{flox/-}$;*p53*$^{-/-}$ MEFs and *Trf1*$^{F/F}$;*Trf2*$^{F/F}$;

Ku70$^{-/-}$;*p53*$^{-/-}$;*Cre-ER*^{T2} MEFs were obtained from T. de Lange[10]. HEK293T cells harboring the DSB-Spectrum_V1 reporter system were a gift from H. van Attikum[38]. HeLa cells with doxycycline-inducible shTRF2 were a gift from J. Lingner[36]. All cells were maintained in Dulbecco's modified Eagle's medium (DMEM) supplemented with 10% fetal calf serum (FCS, Sigma), 100 U ml^{-1} penicillin, 100 µg ml^{-1} streptomycin, and 2 mM L-Glutamine (Gibco, Life Technologies), at 37 °C in a humidified atmosphere with 5% CO_2, except for TRF2ts MEFs, which were cultured at 32 °C. All cell lines were routinely tested for mycoplasma contamination and scored negatively.

FACS-based detection of pKAP1^{S824}

TRF2ts MEFs were trypsinized and resuspended in ice cold PBS/10% FCS, centrifuged at 268 × *g* for 5 min at 4 °C. Cells pellets were resuspended in 0.5 ml ice-cold PBS and fixed while vortexing, by adding dropwise 4.5 ml of ice-cold 100% methanol. Cells were then incubated overnight at −20 °C before starting the staining. After adding 5 ml of PBS, fixed cells were centrifuged for 5 min at 420 × *g*. Cell pellets were resuspended in 500 µl PBS/0.5% BSA (PBA) and cells were permeabilized with 0.1% Triton X-100/PBA on ice for 15 min, followed by 3 washes with PBA and incubation with anti-pKAP1^{S824} antibody (1:250; Bethyl A300-767A) for 3 h at room temperature. After 3 washes with PBA cells were incubated with anti-rabbit Alexa 647 (1:5000, Invitrogen A21246) for 1 h at room temperature. Cells were washed 3 times in PBA and finally resuspended in PBA. FACS was performed with the LSRFortessa Cell Analyzer (BD). FACS data were analyzed by FlowJo 10.4.2 software.

ATD screen

For the ATD screen, a tailored lentiviral shRNA library targeting 123 ubiquitin system factors was assembled from the Mission shRNA library (Sigma). A full list of shRNAs is included in Supplementary Data 2. Infected cells were selected by puromycin, split into triplicates that were each cultured at 39 °C for 3 h and stained for pKAP1^{S824} as described above. The total G1 cell population was FACS-sorted for the 5% cells with the lowest pKAP1 signal, from which the shRNA enrichment was determined relative to the untreated control cell population. Genomic DNA (gDNA) was extracted from the sorted cells using the DNeasy Blood & Tissue Kit (Qiagen). A 2-step PCR recovery of shRNA sequences from gDNA was performed using the Phusion polymerase kit (NEB):

PCR 1:

Thermocycling conditions: (1) 98 °C for 30 s; (2) 20 cycles of 98 °C for 30 s, 60 °C for 30 s, 72 °C for 1 min; (3) 72 °C for 5 min; (4) hold at 4 °C.

Using PCR products from PCR 1 as template for PCR 2:

(1) 98 °C for 30 s; (2) 15 cycles of 98 °C for 30 s, 60 °C for 30 s, 72 °C for 1 min; (3) 72 °C for 5 min; (4) hold at 4 °C.

For primers used in PCR 1 and 2, see Supplementary Data 3.

PCR products from PCR 2 were purified using the Wizard® SV Gel and PCR Clean-Up System (Promega). Purified PCR products were subsequently sequenced using Illumina Hiseq 2500.

shRNA enrichment and gene ranking were done using MAGeCK-RRA analysis[30].

Lentiviral expression constructs and lentiviral packaging

Expression constructs of OTUD5 and KAP1 were used for complementation/rescue experiments. For OTUD5, full-length cDNA of human OTUD5, codon-optimized, was cloned into pCDH-Puro lentiviral expression vector by NheI-EcoRI restriction cloning. Sequence of the codon-optimized cDNA of OTUD5 is included in Supplementary Fig. 5. For KAP1, the expression construct in pLX304-BLAST vector was obtained from the CCSB-Broad Lentiviral Expression Library[72]. Lentiviral particles were packaged as described previously[73], by co-transfecting HEK293T cell with the lentiviral transfer constructs and lentivirus packaging vectors pRRE, pRSV-Rev, pMD2.G. Medium was refreshed once at 16 h post transfection. Lentivirus-containing supernatant was collected at 24–36 h after medium was refreshed.

Site-directed mutagenesis

Mutants of OTUD5 (S177A and C224S) and KAP1 (S824D) were generated by site-directed mutagenesis reactions on pCDH-OTUD5 and pLX304-KAP1 respectively, using the QuikChange II XL directed mutagenesis kit (200521, Agilent) according to manufacturer's instructions. Primers containing the desired mutations were designed using the web based QuikChange Primer Design Program (www.agilent.com/genomics/qcpd). PCR's cycling parameters were as follows: (1) 95 °C for 1 min; (2) 18 cycles of 95 °C for 50 s, 62 °C for 50 s, 68 °C for 12 min; (3) 68 °C for 7 min; (4) hold at 4 °C. The PCR product was treated with 20 U of DpnI enzyme for 2 h at 37 °C to digest the parental/template DNA. The DpnI-treated PCR mix was transformed into Stbl3 *Escherichia coli* (C737303, Thermo Fisher Scientific) following manufacturer's instructions. Transformed cultures were incubated overnight at 37 °C. Mutations were confirmed by Sanger sequencing.

CRISPR/Cas9 gene editing

For CRISPR/Cas9-mediated gene knockout, sgRNA sequences against OTUD5, UBR5, and KAP1 were designed using the Broad Institute's GPP sgRNA Designer (https://portals.broadinstitute.org/gpp/public/analysis-tools/sgrna-design). sgRNA sequences were cloned into a LentiCRISPRv2 plasmid according to standard protocols[33]. Lentiviral particles are packaged as described above[73]. The sgRNA sequences used are included in Supplementary Data 4. LentiCRISPRv2 was a gift from Feng Zhang (Addgene plasmid #52961)[72].

RNA interference

For RNA interference by shRNAs, TRF2ts MEFs were transduced with pLKO.1-puro shRNA lentiviruses from Mission library clones (Sigma). shRNA sequences used for the knockdown of UBE2D3, UBE2M and OTUD5, and their respective Mission library numbers, are included in Supplementary Data 4.

Metaphase chromosome analysis for telomere fusions

Cell collection, preparation of metaphase spreads and telomere FISH with a FITC-OO-$(CCCTAA)_3$ peptide nucleic acid custom probe (Biosynthesis) or Alexa488-labeled C-rich Telomere Probe (Eurogentec) for metaphase chromosome analysis was done as described[27]. Digital images of metaphases were captured using the Metafer4/MSearch automated metaphase finder system (MetaSystems) equipped with an AxioImager Z2 microscope (Carl Zeiss). After scanning metaphase preparations at x10 magnification, high-resolution images of metaphases were acquired using a 'Plan-Apochromat' ×63/1.40 oil objective. Chromosome fusions were quantified from >1500 chromosomes per experimental condition.

Co-Immunoprecipitation

HEK293T cells were transfected with 10 µg of pLVU-GFP-OTUD5 using polyethylenimine. At 16 h post transfection, medium was refreshed. At 48 h post transfection HEK293T cells were lysed in 500 µL of Co-IP Lysis Buffer: 20 mM Tris-HCl pH 7.5, 100 mM NaCl, 1% Nonidet P-40, 5% glycerol, 1 mM EDTA, protease inhibitors (Roche). To complete lysis, cells were incubated for 30 min at 4 °C in a rotating wheel. Lysates were centrifuged for 10 min at 13,523 × *g* and supernatants were collected.

Protein concentration was quantified using Pierce BCA assay (Thermo Fisher Scientific) and lysate containing 2 mg of protein was incubated with 15 µL of washed GFP-Trap® magnetic agarose beads (ChromoTek) overnight at 4 °C in a rotating wheel. Next, beads were washed 3× for 5 min with lysis buffer. For western blot, protein was eluted from beads with 40 µL of 2× SDS sample buffer and incubating at 95 °C for 5 min.

Immunoblotting

Immunoblotting was done according to standard protocols and as described before[29]. Briefly, cells were washed with PBS and collected by scraping in 2× SDS sample buffer followed by boiling at 95 °C. The lysates obtained were sonicated at 30% amplitude for 10 s. Protein concentrations were measured using Pierce BCA Protein Assay (Thermo Fisher Scientific) and equal amounts of protein were loaded onto precast 4–12% Bis-Tris gels (Invitrogen). After protein transfer at 100 V for 60 min onto 0.45 µm nitrocellulose membranes (Amersham), membranes were incubated in blocking buffer and subsequently primary antibodies O/N at 4 °C. Primary antibodies and respective working concentrations are included in Supplementary Data 5. Membranes were incubated with horseradish peroxidase (HRP)-conjugated secondary antibodies (Invitrogen), for detection using enhanced chemiluminescence (SuperSignal West Pico PLUS, Thermo Fisher Scientific) on a Syngene G:BOX, or with IRDye800CW- and IRDye680-labeled secondary antibodies (Li-COR) for detection on the Odyssey CLx Infrared imager (LI-COR). Blots were analyzed using either the GeneSys software (version 1.6.9.0) or the Image Studio Lite LI-COR software (version 5.2.5).

Immunofluorescence

For immunofluorescence, cells were seeded on 15 mm ø coverslips in 12-well plates and treated as indicated in the individual experiments. Cells were washed with PBS, fixed for 10 min with 2% paraformaldehyde followed by 10 min permeabilization in 0.5% Triton/PBS. After 1 h of blocking (0.02% Triton, 5% NGS, 5% FCS in PBS), cells were incubated with primary antibody diluted with blocking solution overnight at 4 °C in a humid chamber. Primary antibodies and respective concentrations used are included in Supplementary Data 5. Next, cells were washed three times with 0.02% Triton/PBS and incubated with Alexa Fluor 488, 568 or 647 goat anti-mouse or anti-rabbit IgG secondary antibodies (Invitrogen) in blocking solution for 1 h at room temperature in the dark. After washing three times with 0.02% Triton/PBS, slides were mounted using ProLong Gold Antifade Mountant with DAPI (Invitrogen). Slides were imaged using a LSM 980 confocal with Airyscan2 system with ×63 oil objective and ZEN software. Image analysis for foci co-localization was performed with the publicly available Foci Analyzer 1.3 macro (https://github.com/BioImaging-NKI/Foci-analyzer) on ImageJ software. Briefly, maximum intensity projections were first produced from Z-stack images. Nuclei were automatically defined using the "Stardist nuclei segmentation". The two channels where the foci were captured were selected for co-localization analysis. Specifically, for the γH2AX-chromocenter co-localization experiment (Fig. 6), the DAPI channel was selected as one of the two channels for co-localization analysis, "Foci size" was set to "large", to enable the detection of chromocenters as foci.

Random plasmid integration assay

For random plasmid integration assays, 500,000 U2OS cells were seeded in 6 cm dishes 24 h before transfection. With the use of Lipofectamine 2000 (Thermo Fisher Scientific) cells were transfected with 3 µg of EcoRI/BamHI-linearized peGFP-C1 plasmid that confers G418 resistance upon successful integration. Transfected cells were trypsinized the following day and seeded in 10 cm dishes at 1000 cells per dish for −G418 controls and 20,000 cells per dish for treatment with G418. Simultaneously, 20,000 cells per sample were seeded separately for assessment of transfection efficiency by the % GFP-positive cells using FACS. Selection was initiated the following day with G418/Geneticin at 500 µg/ml. At 10–14 days after seeding, cells were fixed with 4% paraformaldehyde and stained with 0.1% crystal violet. Dishes were scanned and colony counting was performed using ImageJ (1.52p). NHEJ scores were calculated by normalizing the number of colonies in +G418 dishes to the plating efficiency (-G418) and transfection efficiency (% GFP).

DSB-Spectrum_V1 reporter

The DSB-Spectrum_V1 reporter system was used to assess the NHEJ-HR balance as described[38]. Briefly, DSB-Spectrum_V1 reporter HEK293T cells were seeded at 300,000 cells/well in 12-well plates. The next day, cells were transfected wit pX459-Cas9-sgRNA-mCherry using Lipofectamine 2000 (Invitrogen), according to the manufacturer's protocol. At 48 h post transfection, cells were trypsinized and analyzed by FACS for the % BFP (NHEJ) and % GFP (HR) of transfected (mCherry +) cells using an LSRFortessa Cell Analyzer (BD).

Statistical analysis and reproducibility

Statistical analyses were performed using GraphPad Prism (9.2.0) and Microsoft Excel 2016 (16.0.5356.1000). Details on data representation, statistical tests and number of replicate experiments are indicated in the respective figure legends. Exact p-values are indicated in the figures.

Reporting summary

Further information on research design is available in the Nature Portfolio Reporting Summary linked to this article.

Data availability

All data generated or analyzed during this study are included in this article and its supplementary information files and are available from the corresponding author upon request. Source data are provided with this paper.

References

1. Hanahan, D. & Weinberg, R. A. Hallmarks of cancer: the next generation. *Cell* **144**, 646–674 (2011).
2. Maciejowski, J. & de Lange, T. Telomeres in cancer: tumour suppression and genome instability. *Nat. Rev. Mol. Cell Biol.* **18**, 175–186 (2017).
3. Shay, J. W. & Wright, W. E. Hayflick, his limit, and cellular ageing. *Nat. Rev. Mol. Cell Biol.* **1**, 72–76 (2000).
4. Karlseder, J., Smogorzewska, A. & de Lange, T. Senescence induced by altered telomere state, not telomere loss. *Science* **295**, 2446–2449 (2002).
5. Denchi, E. L. & de Lange, T. Protection of telomeres through independent control of ATM and ATR by TRF2 and POT1. *Nature* **448**, 1068–1071 (2007).
6. Bae, N. S. & Baumann, P. A RAP1/TRF2 complex inhibits nonhomologous end-joining at human telomeric DNA ends. *Mol. Cell* **26**, 323–334 (2007).
7. Lazzerini-Denchi, E. & Sfeir, A. Stop pulling my strings - what telomeres taught us about the DNA damage response. *Nat. Rev. Mol. Cell Biol.* **17**, 364–378 (2016).
8. van Steensel, B., Smogorzewska, A. & de Lange, T. TRF2 protects human telomeres from end-to-end fusions. *Cell* **92**, 401–413 (1998).
9. Stansel, R. M., de Lange, T. & Griffith, J. D. T-loop assembly in vitro involves binding of TRF2 near the 3′ telomeric overhang. *EMBO J.* **20**, 5532–5540 (2001).
10. Sfeir, A. & de Lange, T. Removal of shelterin reveals the telomere end-protection problem. *Science* **336**, 593–597 (2012).
11. Uziel, T. et al. Requirement of the MRN complex for ATM activation by DNA damage. *EMBO J.* **22**, 5612–5621 (2003).
12. Blackford, A. N. & Jackson, S. P. ATM, ATR, and DNA-PK: the trinity at the heart of the DNA damage response. *Mol. Cell* **66**, 801–817 (2017).
13. Banin, S. et al. Enhanced phosphorylation of p53 by ATM in response to DNA damage. *Science* **281**, 1674–1677 (1998).
14. Matsuoka, S. et al. Ataxia telangiectasia-mutated phosphorylates Chk2 in vivo and in vitro. *Proc. Natl Acad. Sci. USA* **97**, 10389–10394 (2000).
15. Burma, S., Chen, B. P., Murphy, M., Kurimasa, A. & Chen, D. J. ATM phosphorylates histone H2AX in response to DNA double-strand breaks. *J. Biol. Chem.* **276**, 42462–42467 (2001).

16. Ziv, Y. et al. Chromatin relaxation in response to DNA double-strand breaks is modulated by a novel ATM- and KAP-1 dependent pathway. *Nat. Cell Biol.* **8**, 870–876 (2006).
17. Goodarzi, A. A. et al. ATM signaling facilitates repair of DNA double-strand breaks associated with heterochromatin. *Mol. Cell* **31**, 167–177 (2008).
18. Noon, A. T. et al. 53BP1-dependent robust localized KAP-1 phosphorylation is essential for heterochromatic DNA double-strand break repair. *Nat. Cell Biol.* **12**, 177–184 (2010).
19. Goodarzi, A. A., Kurka, T. & Jeggo, P. A. KAP-1 phosphorylation regulates CHD3 nucleosome remodeling during the DNA double-strand break response. *Nat. Struct. Mol. Biol.* **18**, 831–839 (2011).
20. Schwertman, P., Bekker-Jensen, S. & Mailand, N. Regulation of DNA double-strand break repair by ubiquitin and ubiquitin-like modifiers. *Nat. Rev. Mol. Cell Biol.* **17**, 379–394 (2016).
21. Mailand, N. et al. RNF8 ubiquitylates histones at DNA double-strand breaks and promotes assembly of repair proteins. *Cell* **131**, 887–900 (2007).
22. Doil, C. et al. RNF168 binds and amplifies ubiquitin conjugates on damaged chromosomes to allow accumulation of repair proteins. *Cell* **136**, 435–446 (2009).
23. Poulsen, M., Lukas, C., Lukas, J., Bekker-Jensen, S. & Mailand, N. Human RNF169 is a negative regulator of the ubiquitin-dependent response to DNA double-strand breaks. *J. Cell Biol.* **197**, 189–199 (2012).
24. Huang, O. W. et al. Phosphorylation-dependent activity of the deubiquitinase DUBA. *Nat. Struct. Mol. Biol.* **19**, 171–175 (2012).
25. de Vivo, A. et al. The OTUD5-UBR5 complex regulates FACT-mediated transcription at damaged chromatin. *Nucleic Acids Res.* **47**, 729–746 (2019).
26. Zhang, T., Cronshaw, J., Kanu, N., Snijders, A. P. & Behrens, A. UBR5-mediated ubiquitination of ATMIN is required for ionizing radiation-induced ATM signaling and function. *Proc. Natl Acad. Sci. USA* **111**, 12091–12096 (2014).
27. Konishi, A. & de Lange, T. Cell cycle control of telomere protection and NHEJ revealed by a ts mutation in the DNA-binding domain of TRF2. *Genes Dev.* **22**, 1221–1230 (2008).
28. Sakaue-Sawano, A. & Miyawaki, A. Visualizing spatiotemporal dynamics of multicellular cell-cycle progressions with fucci technology. *Cold Spring Harb. Protoc.* **2014**, https://doi.org/10.1101/pdb.prot080408 (2014).
29. Boersma, V. et al. MAD2L2 controls DNA repair at telomeres and DNA breaks by inhibiting 5′ end resection. *Nature* **521**, 537–540 (2015).
30. Li, W. et al. MAGeCK enables robust identification of essential genes from genome-scale CRISPR/Cas9 knockout screens. *Genome Biol.* **15**, 554 (2014).
31. Yalcin, Z. et al. UBE2D3 facilitates NHEJ by orchestrating ATM signalling through multi-level control of RNF168. *Nat. Commun.* **15**, 5032 (2024).
32. Enchev, R. I., Schulman, B. A. & Peter, M. Protein neddylation: beyond cullin-RING ligases. *Nat. Rev. Mol. Cell Biol.* **16**, 30–44 (2015).
33. Sanjana, N. E., Shalem, O. & Zhang, F. Improved vectors and genome-wide libraries for CRISPR screening. *Nat. Methods* **11**, 783–784 (2014).
34. Smogorzewska, A., Karlseder, J., Holtgreve-Grez, H., Jauch, A. & de Lange, T. DNA ligase IV-dependent NHEJ of deprotected mammalian telomeres in G1 and G2. *Curr. Biol.* **12**, 1635–1644 (2002).
35. Celli, G. B., Denchi, E. L. & de Lange, T. Ku70 stimulates fusion of dysfunctional telomeres yet protects chromosome ends from homologous recombination. *Nat. Cell Biol.* **8**, 885–890 (2006).
36. Grolimund, L. et al. A quantitative telomeric chromatin isolation protocol identifies different telomeric states. *Nat. Commun.* **4**, 2848 (2013).
37. Ahnesorg, P., Smith, P. & Jackson, S. P. XLF interacts with the XRCC4-DNA ligase IV complex to promote DNA nonhomologous end-joining. *Cell* **124**, 301–313 (2006).
38. van de Kooij, B., Kruswick, A., van Attikum, H. & Yaffe, M. B. Multi-pathway DNA-repair reporters reveal competition between end-joining, single-strand annealing and homologous recombination at Cas9-induced DNA double-strand breaks. *Nat. Commun.* **13**, 5295 (2022).
39. Li, F. et al. The deubiquitinase OTUD5 regulates Ku80 stability and non-homologous end joining. *Cell Mol. Life Sci.* **76**, 3861–3873 (2019).
40. Nishi, R. et al. The deubiquitylating enzyme UCHL3 regulates Ku80 retention at sites of DNA damage. *Sci. Rep.* **8**, 17891 (2018).
41. Dimitrova, N., Chen, Y. C., Spector, D. L. & de Lange, T. 53BP1 promotes non-homologous end joining of telomeres by increasing chromatin mobility. *Nature* **456**, 524–528 (2008).
42. Zimmermann, M., Lottersberger, F., Buonomo, S. B., Sfeir, A. & de Lange, T. 53BP1 regulates DSB repair using Rif1 to control 5′ end resection. *Science* **339**, 700–704 (2013).
43. Chapman, J. R. et al. RIF1 is essential for 53BP1-dependent non-homologous end joining and suppression of DNA double-strand break resection. *Mol. Cell* **49**, 858–871 (2013).
44. Di Virgilio, M. et al. Rif1 prevents resection of DNA breaks and promotes immunoglobulin class switching. *Science* **339**, 711–715 (2013).
45. Escribano-Diaz, C. et al. A cell cycle-dependent regulatory circuit composed of 53BP1-RIF1 and BRCA1-CtIP controls DNA repair pathway choice. *Mol. Cell* **49**, 872–883 (2013).
46. Friedman, J. R. et al. KAP-1, a novel corepressor for the highly conserved KRAB repression domain. *Genes Dev.* **10**, 2067–2078 (1996).
47. Moosmann, P., Georgiev, O., Le Douarin, B., Bourquin, J. P. & Schaffner, W. Transcriptional repression by RING finger protein TIF1 beta that interacts with the KRAB repressor domain of KOX1. *Nucleic Acids Res.* **24**, 4859–4867 (1996).
48. White, D. et al. The ATM substrate KAP1 controls DNA repair in heterochromatin: regulation by HP1 proteins and serine 473/824 phosphorylation. *Mol. Cancer Res.* **10**, 401–414 (2012).
49. Cubiles, M. D. et al. Epigenetic features of human telomeres. *Nucleic Acids Res.* **46**, 2347–2355 (2018).
50. Garcia-Cao, M., O'Sullivan, R., Peters, A. H., Jenuwein, T. & Blasco, M. A. Epigenetic regulation of telomere length in mammalian cells by the Suv39h1 and Suv39h2 histone methyltransferases. *Nat. Genet.* **36**, 94–99 (2004).
51. Bartocci, C. et al. Isolation of chromatin from dysfunctional telomeres reveals an important role for Ring1b in NHEJ-mediated chromosome fusions. *Cell Rep.* **7**, 1320–1332 (2014).
52. Dejardin, J. & Kingston, R. E. Purification of proteins associated with specific genomic Loci. *Cell* **136**, 175–186 (2009).
53. Lin, C. G. et al. The human telomeric proteome during telomere replication. *Nucleic Acids Res.* **49**, 12119–12135 (2021).
54. Cho, J. H. et al. Deubiquitinase OTUD5 is a positive regulator of mTORC1 and mTORC2 signaling pathways. *Cell Death Differ.* **28**, 900–914 (2021).
55. Hou, T. et al. Deubiquitinase OTUD5 modulates mTORC1 signaling to promote bladder cancer progression. *Cell Death Dis.* **13**, 778 (2022).
56. Kim, S. T., Lim, D. S., Canman, C. E. & Kastan, M. B. Substrate specificities and identification of putative substrates of ATM kinase family members. *J. Biol. Chem.* **274**, 37538–37543 (1999).
57. Traven, A. & Heierhorst, J. SQ/TQ cluster domains: concentrated ATM/ATR kinase phosphorylation site regions in DNA-damage-response proteins. *Bioessays* **27**, 397–407 (2005).
58. Schlam-Babayov, S. et al. Phosphoproteomics reveals novel modes of function and inter-relationships among PIKKs in response to genotoxic stress. *EMBO J.* **40**, e104400 (2021).

59. Vancevska, A., Douglass, K. M., Pfeiffer, V., Manley, S. & Lingner, J. The telomeric DNA damage response occurs in the absence of chromatin decompaction. *Genes Dev.* **31**, 567–577 (2017).
60. Timashev, L. A., Babcock, H., Zhuang, X. & de Lange, T. The DDR at telomeres lacking intact shelterin does not require substantial chromatin decompaction. *Genes Dev.* **31**, 578–589 (2017).
61. Kubben, N. et al. Identification of differential protein interactors of lamin A and progerin. *Nucleus* **1**, 513–525 (2010).
62. Neumann-Staubitz, P., Kitsberg, D., Buxboim, A. & Neumann, H. A method to map the interaction network of the nuclear lamina with genetically encoded photo-crosslinkers in vivo. *Front. Chem.* **10**, 905794 (2022).
63. Crabbe, L., Cesare, A. J., Kasuboski, J. M., Fitzpatrick, J. A. & Karlseder, J. Human telomeres are tethered to the nuclear envelope during postmitotic nuclear assembly. *Cell Rep.* **2**, 1521–1529 (2012).
64. Wood, A. M., Laster, K., Rice, E. L. & Kosak, S. T. A beginning of the end: new insights into the functional organization of telomeres. *Nucleus* **6**, 172–178 (2015).
65. Gonzalez-Sandoval, A. & Gasser, S. M. On TADs and LADs: spatial control over gene expression. *Trends Genet.* **32**, 485–495 (2016).
66. Zong, D., Oberdoerffer, P., Batista, P. J. & Nussenzweig, A. RNA: a double-edged sword in genome maintenance. *Nat. Rev. Genet.* **21**, 651–670 (2020).
67. Lottersberger, F., Karssemeijer, R. A., Dimitrova, N. & de Lange, T. 53BP1 and the LINC complex promote microtubule-dependent DSB mobility and DNA repair. *Cell* **163**, 880–893 (2015).
68. Hu, M. et al. Expression of KAP1 in epithelial ovarian cancer and its correlation with drug-resistance. *Int. J. Clin. Exp. Med.* **8**, 17308–17320 (2015).
69. Cui, Y. et al. High levels of KAP1 expression are associated with aggressive clinical features in ovarian cancer. *Int. J. Mol. Sci.* **16**, 363–377 (2014).
70. Yokoe, T. et al. KAP1 is associated with peritoneal carcinomatosis in gastric cancer. *Ann. Surg. Oncol.* **17**, 821–828 (2010).
71. Peuscher, M. H. & Jacobs, J. J. DNA-damage response and repair activities at uncapped telomeres depend on RNF8. *Nat. Cell Biol.* **13**, 1139–1145 (2011).
72. Yang, X. et al. A public genome-scale lentiviral expression library of human ORFs. *Nat. Methods* **8**, 659–661 (2011).
73. de Krijger, I. et al. MAD2L2 dimerization and TRIP13 control shieldin activity in DNA repair. *Nat. Commun.* **12**, 5421 (2021).

Acknowledgements

We thank Titia de Lange for TRF2^{I468A} expression vector and *Trf2*$^{flox/-}$;*p53*$^{-/-}$ MEFs, used to generate TRF2ts MEFs, and for *Trf1*$^{F/F}$;*Trf2*$^{F/F}$;*Ku70*$^{-/-}$;*p53*$^{-/-}$;*Cre-ER*^{T2} MEFs. We thank Haico van Attikum and Bert van der Kooij for HEK293T cells with the DSB-Spectrum_V1 reporter, Joachim Lingner for the HeLa shTRF2 cells, Thomas Kuilman for MAGeCK-RRA analysis of the screen results, Daniëlle Koot for assistance with IF-FISH and Brigitte Wevers for contributing to initial optimization of the pKAP1 screen. This work was supported by the European Union's Horizon 2020 research and innovation program (Marie-Skłodowska-Curie grant agreement 812829) to J.J.L.J, Dutch Cancer Society project grant KWF 2019-2/12826 to J.J.L.J., and an institutional grant of the Dutch Cancer Society and the Dutch Ministry of Health, Welfare and Sport to the Netherlands Cancer Institute.

Author contributions

J.J.L.J. conceived the original idea for the screen and together with S.Y.L. and R.v.d.L. conceived the ideas for follow-up work. M.S. constructed the shRNA library and A.C. conducted the screen. S.Y.L. and R.v.d.L. performed most experiments, Z.Y. assessed telomere fusion upon UBR5 knockdown and A.T. conducted DSB-spectrum_V1 reporter assays. J.J.L.J. and S.Y.L. co-wrote the manuscript, to which R.v.d.L. contributed with comments, composing part of the figures and responding to peer reviewers.

Competing interests

The authors declare no competing interests.

Additional information

Supplementary information The online version contains supplementary material available at https://doi.org/10.1038/s41467-024-53404-0.

Correspondence and requests for materials should be addressed to Jacqueline J. L. Jacobs.

Peer review information *Nature Communications* thanks Younghoon Kee, Tej Pandita, and the other, anonymous, reviewer(s) for their contribution to the peer review of this work. A peer review file is available.